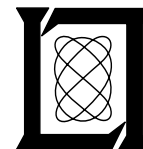# Preliminary Results of the 1983 Coordinated Aircraft – Doppler Weather Radar Turbulence Experiment, Volume 1

Y. Lee
A. R. Paradis
D. Klingle-Wilson

26 July 1988

Lincoln Laboratory

MASSACHUSETTS INSTITUTE OF TECHNOLOGY

LEXINGTON, MASSACHUSETTS

1. Report No.	2. Government Accession No.	3. Recipient's Catalog No.
DOT/FAA/PM-86/11		

4. Title and Subtitle	5. Report Date
Preliminary Results of the 1983 Coordinated Aircraft — Doppler Weather Radar Turbulence Experiment, Volume I	26 July 1988
	6. Performing Organization Code

7. Author(s)	8. Performing Organization Report No.
Yean Lee, Albert R. Paradis, and Diana Klingle-Wilson	ATC-137

9. Performing Organization Name and Address	10. Work Unit No. (TRAIS)
Lincoln Laboratory, MIT P.O. Box 73 Lexington, MA 02173-0073	
	11. Contract or Grant No.
	DT-FA01-80-Y-10546
	13. Type of Report and Period Covered

12. Sponsoring Agency Name and Address	
Department of Transportation Federal Aviation Administration Systems Research and Development Service Washington, DC 20591	Project Report
	14. Sponsoring Agency Code

15. Supplementary Notes

16. Abstract

This report presents results of analyses of coordinated radar-aircraft data acquired from the 1983 experiment conducted at Hanscom AFB, Massachusetts. The objective of the experiment is to assess and validate the current NEXRAD algorithms for estimating aircraft turbulence from volume-scanned Doppler weather radar observations. Estimates of the turbulence severity index $\epsilon^{1/3}$ (a quantity used by NEXRAD) computed from radar and aircraft data are presented as a time series along each aircraft track. The radar point estimates of turbulence were averaged horizontally and vertically to yield layered Cartesian maps such as are intended for use by real time ATC controllers and pilots. The derived gust velocity (Ude), also used to indicate the intensity of aircraft encountered turbulence, was computed so that comparisons could be made of the turbulence intensity scales inferred from values of $\epsilon^{1/3}$ and U_{de}.

These quantitative comparisons indicate that for the turbulence generally encountered during the flights, both radar and aircraft estimates of $\epsilon^{1/3}$ significantly overstate the severity of turbulence as reported by the aircraft pilot. The data analysis also shows that radar-based estimates of $\epsilon^{1/3}$, often significantly exceeded aircraft based estimates of $\epsilon^{1/3}$. In contrast, the quantity Ude underestimates the aircraft reported turbulence intensity on all the flights. The uncertainty as to operationally useful thresholds for radar $\epsilon^{1/3}$, aircraft $\epsilon^{1/3}$ and U_{de} is discussed as is the use of spectrum width as a turbulence indicator.

It should be noted that the turbulence detection flights used in the study were conducted at ranges such that the radar resolution cell cross range extent was typically 1.5 to 3 km. With such resolution cell size extents, the hypothesis of spatially homogeneous turbulence may not hold and/or the assumed relationship of radar measured spectrum width to kinetic dissipation rate may not be fully accurate.

17. Key Words		18. Distribution Statement
Doppler weather radar aircraft turbulence Doppler spectrum width turbulence detection turbulence severity index	turbulence intensity scale kinetic energy dissipation rate derived gust velocity NEXRAD	Document is available to the public through the National Technical Information Service, Springfield, VA 22161.

19. Security Classif. (of this report)	20. Security Classif. (of this page)	21. No. of Pages	22. Price
Unclassified	Unclassified	76	

FORM DOT F 1700.7 (8-69)

List of Errors:

pg.5 Definitions concerning equation (2) are incorrect. γ (ratio of specific heats is written as "g". τ is written as "t".

pg.6 Definitions concerning equation (3) are incorrect. Units on D_a are wrong. Air density ρ is written as "r".

pg.8 Equation (7) should read $D_a^{1/2}$ instead of D_a.

The following sentence should read "... comparing Eqs. (3) and (5)..." rather than "...(3) and (4)...".

U_{de} is inversely proportional to V.

The text states that ϵ_a is directly proportional to $V^{4/3}$. In fact, it is $\epsilon_a^{1/3}$ that is inversely proportional to $V^{4/3}$.

In the following paragraph, the text should read "... whereas $D_a^{1/2}$ will be ..." rather than "...$D_a^{1/3} \cdots$".

pg.22 Second paragraph: Text should read "(see Figure 2 and Table 4)", not "... Figure 3 and Table 5...".

2nd paragraph: I see no support for the statement that "peak values of $\epsilon_p^{1/3}$ or $\epsilon_a^{1/3}$...indicate 'extreme' turbulence" even using the MacCready intensity scale. Indeed if the more conservative Bohne scale is used, the $\epsilon^{1/3}$ measurements indicate the same "moderate" turbulence levels indicated by the pilots.

2nd paragraph: What is D_g? This parameter is never defined and never mentioned aside from this paragraph.

pg.25 The summary for Section 2 states that $\epsilon_a^{1/3}$ overstates turbulence intensity relative to pilot reports. The data presented in the chapter and the statement on page 12 indicate that it is $\epsilon_p^{1/3}$ that is the greater offender in terms of overestimation of turbulence severity.

pg.26 In equation (8) a conversion factor is written once as C_F and once as CF.

Equation (8) uses "mixed" units. A spectrum width expressed in m/s, divided by the cube root a range expressed in kilometers will not give $\epsilon_r^{1/3}$ in $(cm^{2/3}sec^{-1})$. Indeed, throughout the report, the authors switch between CGS and MKS units and occasional mixtures of the two.

pg.28 In Table 12, "rotation" is spelled "roataion".

pg.31 Last paragraph: "...corroborated by Table 4..." should read "...Table 5...".

pg.45 Caption for Table 18 should read "...aircraft-acceleration structure function...", not "...aircraft-pressure structure function...".

pg.60 Second paragraph: Should read "(see Figure 6)", not "(see Figure 5)".

ABSTRACT

This report presents results of analyses of coordinated radar–aircraft data acquired from the 1983 experiment conducted at Hanscom AFB, Massachusetts. The objective of the experiment is to assess and validate the current NEXRAD algorithms for estimating aircraft turbulence from volume–scanned Doppler weather radar observations. Estimates of the turbulence severity index $\epsilon^{1/3}$ (a quantity used by NEXRAD) computed from radar and aircraft data are presented as a time series along each aircraft track. The radar point estimates of turbulence were averaged horizontally and vertically to yield layered Cartesian maps such as are intended for use by real time ATC controllers and pilots. The derived gust velocity (Ude), also used to indicate the intensity of aircraft encountered turbulence, was computed so that comparisons could be made of the turbulence intensity scales inferred from values of $\epsilon^{1/3}$ and U_{de}.

These quantitative comparisons indicate that for the turbulence generally encountered during the flights, both radar and aircraft estimates of $\epsilon^{1/3}$ significantly overstate the severity of turbulence as reported by the aircraft pilot. The data analysis also shows that radar–based estimates of $\epsilon^{1/3}$, often significantly exceeded aircraft based estimates of $\epsilon^{1/3}$. In contrast, the quantity Ude underestimates the aircraft reported turbulence intensity on all the flights. The uncertainty as to operationally useful thresholds for radar $\epsilon^{1/3}$, aircraft $\epsilon^{1/3}$ and U_{de} is discussed as is the use of spectrum width as a turbulence indicator.

It should be noted that the turbulence detection flights used in the study were conducted at ranges such that the radar resolution cell cross range extent was typically 1.5 km to 3 km. With such resolution cell size extents, the hypothesis of spatially homogeneous turbulence may not hold and/or the assumed relationship of radar measured spectrum width to kinetic dissipation rate may not be fully accurate.

ACKNOWLEDGEMENTS

CONTENTS

LIST OF ACRONYMS

AFGL	Air Force Geophysics Laboratory
ATC	Air Traffic Control
ATCRBS	Air Traffic Control Radar Beacon System
CPI	Coherent Processing Interval
CWP	Central Weather Processor
FAA	Federal Avaition Administration
GMT	Greenwich Mean Time
INS	Inertial Navigation System
JSPO	Joint System Program Office
MIT	Massachusetts Institute of Technology
NEXRAD	Next Generation Weather Radar
NTR	NEXRAD Technical Requirements
PPI	Plan Position Indicator
RF	Radio Frequency
RHI	Range Height Indicator
STC	Sensitivity Time Control
TDWR	Terminal Doppler Weather Radar
TOS	Turbulence Outer Scale
TSI	Turbulence Severity Index
UND	University of North Dakota

LIST OF FIGURES

LIST OF TABLES

1. INTRODUCTION

Studies have shown that atmospheric turbulence is an important hazard in thunderstorms. It is a direct cause of many aircraft accidents and an important factor in many others (Thomas, 1971). Accordingly, improved turbulence detection has been a principal objective of the Federal Aviation Administration (FAA) weather radar program for a number of years. During the summer of 1983, a series of coordinated instrumented aircraft/Doppler weather radar field experiments were conducted near Hanscom Air Force Base, Massachusetts. The program objectives relevant to turbulence detection were 1) to obtain and analyze aircraft and radar turbulence measurements, and 2) to validate and improve the currently existing turbulence algorithms in the context of the anticipated FAA use of these data to provide real time warning of hazardous aviation weather to FAA Air Traffic Control (ATC) users (*e.g.*, controllers and pilots).

This report presents results from the coordinated aircraft/radar turbulence data acquisition program. Volume 1 of this report discusses the experiment and briefly reviews the relevant theory. Selected results are presented which illustrate a number of issues associated with the practical implementation of turbulence detection algorithms applicable in the context of NEXRAD (Next Generation Weather Radar) and TDWR (Terminal Doppler Weather Radar) systems. Volume 2 is a compilation of the results from all the experimental flights of the 1983 program.

The parameter of primary interest in characterizing the intensity of atmospheric turbulence is the turbulent kinetic energy dissipation rate ϵ. In particular ϵ provides a statistical measure of turbulent activity associated with regions of isotropic, homogeneous turbulence. Since it can be shown that $\epsilon^{1/3}$ (termed turbulence severity index by Bohne, 1982) is directly proportional to the rms (root mean square) vertical acceleration of an aircraft, maps of $\epsilon^{1/3}$ can identify hazardous regions of airspace. Moreover, since this parameter intrinsically reflects the storm environment and not the sensor characteristics it can serve as the basis for a universal turbulence intensity scale.

The turbulence encountered by a plane can be estimated in several ways. *In situ* aircraft measurements of the spatial fluctuations in air pressure and aircraft vertical accelerations provide two independent mechanisms for estimating $\epsilon^{1/3}$, as discussed in Section 2 of this volume which describes the methods suggested by Labitt (1981). The derived gust velocity, U_{de}, is another parameter used to indicate turbulence intensity based on aircraft acceleration measurements. It is also discussed in Section 2.

There are several approaches to the estimation of $\epsilon^{1/3}$ from Doppler radar observations of the atmosphere. The current NEXRAD algorithm for turbulence detection, due to Bohne of the Air Force Geophysics Laboratory (AFGL), estimates the turbulence severity index from the Doppler spectral variance (Bohne, 1982; NEXRAD JSPO, 1985). We consider both Bohne's algorithm and an earlier similar algorithm due to Labitt (1981). Section 3 compares time series of aircraft-estimated $\epsilon_a^{1/3}$ and U_{de} with a corresponding time series of radar-estimated $\epsilon_r^{1/3}$ along the flight path. These quantitative comparisons indicate to what extent radar-based turbulence estimates correlate with the aircraft turbulence measurements, and indicate if the radar spectral variance estimates (obtained by the pulse pair covariance technique) can be used to reliably estimate the kinetic energy dissipation rate ϵ associated with convective storm systems.

Previous turbulence detection experiments have compared the aircraft data with radar estimates which were in close proximity spatially and temporally to the aircraft data. However, the FAA plans to provide turbulence detection results from NEXRAD in real time to nonmeteorologist and ATC users by:

(1) using the radar measurements from a number of elevation angles of a NEXRAD volume scan to estimate the turbulence in several altitude layers (corresponding to the altitude sectors used for enroute ATC), and

(2) mosaicing the results from the various NEXRAD radars, which cover the airspace of concern, in the Central Weather Processor (CWP) to yield turbulent region maps for distribution.

As a result of these operational considerations, the NEXRAD/CWP-based turbulence estimates will be displaced in time from the actual aircraft turbulence encounters as well as representing a spatial average over a sizable region (*e.g.*, 4 km x 4 km x 4 km to 8 km) about the aircraft.

The aircraft turbulence results are compared with radar derived layered reflectivity, spectrum width and dissipation rate maps to ascertain the reliability of the estimates in the ATC operational context described above. The effect of varying the layer spatial scale on turbulence detection performance is assessed by comparing results with various layer dimensions to the aircraft flight data.

The final section discusses the principal results and makes suggestions for future work in this area.

2. AIRCRAFT OBSERVATIONS

The aircraft used was the University of North Dakota's (UND) Cessna Citation II, a twin-engine fanjet instrumented for cloud physics and meteorological research. The instrumentation for measuring relevant parameters used in this report are listed in Table 1. The principal meteorological variables sensed were the absolute and the differential pressure, temperature, and humidity. In addition, the aircraft was equipped with an Inertial Navigation System (INS) including a three-axis accelerometer to provide a measure of relative turbulence level. All of the sensor outputs are digitally recorded with a sampling interval of $T_S=1/24$ sec. The data were prefiltered over one second intervals.

The quantities $\epsilon^{1/3}$ and U_{de} have been used by many investigators, but their interests were focused on either one or the other. So far no simultaneous comparison of $\epsilon^{1/3}$ and U_{de} from the same set of aircraft data has appeared. This report presents measurements of the temporal variation of these quantities along the same level flight path. By comparing the results, we examine not only the similiarity between the two quantities but also whether the suggested turbulence magnitude scales are able to reflect the turbulence severity subjectively reported by the pilot.

2.1 Estimation of Kinetic Energy Dissipation Rate Parameter

The use of kinetic energy dissipation rate as a turbulence indicator arises from considering the turbulence to be a spatially homogeneous, random field. The main characteristic of atmospheric turbulent motion considered as a random process is the disorder of the velocity field in both space and time. An observed velocity u(t) can be considered a realization from an ensemble with mean $\bar{u}(t)$, which is usually interpreted as the mean wind on which the turbulent component $\tilde{u}(t) = u(t)-\bar{u}(t)$ is superimposed. The numerical value of a quantity such as $E[\tilde{u}^2(t)]$ is a measure of turbulent energy. According to Kolmogorov's turbulence theory, (as described by Bachelor, 1960) energy is transferred from the largest eddies to the smallest and is ultimately dissipated as heat by viscosity at the smallest eddies.

If the turbulence is homogeneous and isotropic over a certain range of eddy sizes, the turbulent energy distribution has a spatial energy density which decreases with wavenumber according to a −5/3 power law. This range of eddy sizes is known as the inertial subrange defined in the similarity hypothesis of Kolmogorov. Wavenumbers which are smaller than the inertial subrange correspond to spatial scales in which the turbulence energy is generated by large-scale nonhomogeneous processes such as vertical shear. According to Kolmogorov's hypothesis, in the inertial subrange energy is transferred from eddy size to eddy size without loss. Therefore, the rate of energy transfer from one-scale to a smaller one must be numerically equal to the rate of kinetic energy dissipation $\epsilon(cm^2/sec^3)$. Thus the spectrum of the turbulent velocity field is determined by the quantity ϵ and a nondimensional constant. The value of ϵ can be calculated from the energy spectral density if the spectrum for any wavenumber belonging to the inertial subrange is known.

An alternative mechanism for estimating ϵ is based on the use of structure functions. The structure function associated with a random field is defined as the expectation of the square of the difference between field values at different locations and/or different times:

Table 1. UND Citation Instrumentation Specifications

PARAMETER MEASURED	INSTRUMENT TYPE	MANUFACTURER & MODEL NO.	RANGE	RESPONSE TIME	ACCURACY	RESOLUTION
Temperature	Platinum Resistance	Rosemount Engineering Co. 510 B Signal Conditioner & Model 102 Probe	± 50 °C	1 sec	± 0.5 °C	0.1°C
Altitude	INS and Static Press	Litton LTN–76	0 to 45 kft	–	uncertain due to lack of standard	2m
Indicated Air Speed	Differential Pressure	Rosemount 858AJ	0 to 5 psid	0.3 msec	0.005 psid	0.003 psid
Vertical Acceleration	Inertial Navigation System	Litton LTN–76 (with dual Speed Resolvers)	+3 to −1 G	42 msec update	± 0.01G	0.001G
Position	Inertial Navigation System	Litton LTN–76 (with dual Speed Resolvers)	–	42 msec update	± 1. Naut mi (without update)	60 ft
Static Pressure		Rosemount 858AJ				

I
4
I

$$D_x = E\{[\ x(r + \Delta r) - x(r)]^2\}$$
(1)

where the random field x is measured at locations separated by the distance vector Δr. In this study, the aircraft-based computations of ϵ are developed from both a pressure structure function and an acceleration structure function.

As pointed out by Labitt (1981), there is a theoretical relationship among the pitot differential pressure, its structure function, absolute pressure, and the kinetic energy dissipation rate (ϵ). The relationship can be written as:

$$\epsilon_p^{1/3} = \frac{\left(\dfrac{RT_t}{\tau}\right)^{1/3} \left(\dfrac{\gamma-1}{2\gamma}\right)^{2/3} \sqrt{D_{\Delta p}}}{C^{1/2} \cdot \left(1 + \dfrac{\Delta p}{P_f}\right)^{\frac{\gamma+2}{3\gamma}} \cdot \left[\left(1 + \dfrac{\Delta p}{P_f}\right)^{\frac{\gamma-1}{\gamma}} - 1\right]^{2/3} \cdot P_f}$$
(2)

where the Δp structure function is defined as:

$$D_{\Delta p} = E\{[\Delta p(t + \tau) - \Delta p(t)]^2\}$$

$$\Delta P = P_t - P_f$$

P_t = total pressure

P_f = static pressure

T_t = total temperature

R = 2.87 x 10^6 cm²/sec/K

γ = 1.4 (ratio of specific heats)

τ = 1.0 sec (time between successive Δp measurements),

C = Kolmogorov's constant (1.77 ± .08)

The quantity ϵ can also be estimated from the acceleration structure function and the airspeed, using the formula derived by Labitt (1981):

$$\epsilon_a^{1/3} = \left[\frac{3D_a}{C}\right]^{1/2} \frac{m}{C_{L_\alpha} \ S \ \rho \ V_t^{4/3} \ \tau^{1/3}} \quad (cm^{2/3} sec^{-1})$$
(3)

where:

D_a = acceleration structure function (cm/sec^2)

D_a = E { $[a(t+\tau) - a(t)]^2$}

$a(t)$ = vertical acceleration of the aircraft

V_t = true airspeed (cm/sec)

ρ = air density at flight level (gm/cm^3)

m = aircraft mass (gm)

$C_{L\alpha}$ = aircraft lift curve slope

S = wing area (cm^2)

τ = sampling time interval (sec)

C = Kolmogorov's constant (1.77 $\pm$ .08)

For the Cessna Citation II:

$C_{L\alpha}$ = 6.1 (radians^{-1})

S = 300000 cm^2

m = 5585085.5 gm

2.2 Evaluation of Derived Gust Velocity

Alternatively, we may regard the flight of an aircraft in a turbulent environment as being perturbed by discrete deterministic gusts. It is clear that an aircraft does not react to gusts of all spatial sizes, but only to a comparatively narrow part of the entire spectrum of turbulence that affects the flight conditions. For instance, low-frequency turbulence may carry the airplane upward or downward without appreciably changing its loads*. In contrast, high-frequency turbulence may lead to such small loads that they are practically unnoticed. Thus, the load variations experienced by aircraft depend both on the intensity of the turbulence and its spatial characteristics.

The following formula relates the load increment to the intensity of a "worst" case vertical gust characterized by the so-called derived gust velocity U_{de}. The gust velocity of the assumed one-minus-cosine gust is:

$$V_g(t) = \frac{1}{2} U_{de}\left[1 - Cos\frac{2\pi V_e t}{25\bar{c}}\right] \tag{4}$$

----

* An aircraft load is defined as the ratio of the lift force to the weight. When the ratio is 1, it implies that the aircraft is in calm horizontal flight.

where:

$V_g(t) =$ Vertical gust velocity

$U_{de} =$ Maximum vertical gust velocity

$V_e =$ Equivalent airspeed of aircraft

$\bar{c} =$ Mean aerodynamic chord

Using Eq. (4) and standard aircraft single degree of freedom modeling, it can be shown that the aircraft vertical acceleration (A_n) due to the gust is related to U_{de} by:

$$U_{de} = \frac{2 \mid A_n \mid m}{V_i \, K_g \, \rho_o \, C_{L_\alpha} \, S} \quad \text{(m/sec)} \tag{5}$$

where:

$A_n =$ incremental vertical acceleration of aircraft (from normal)

$m =$ aircraft mass (gm)

$V_i =$ indicated air speed (m/sec)

$K_g =$ gust factor (0.88)

$\rho_o =$ air density at sea level (gm/m^3)

$C_{L_\alpha} =$ aircraft lift curve slope

The indicated (V_i) and true airspeed (V_t) are related by:

$$V_t = V_i \, (\rho_o / \rho)^{1/2} \tag{6}$$

where ρ_o is the density of air at sea level of the standard atmosphere and ρ is the density of the air through which the aircraft is flying.

2.3 Applications of Turbulence Measures to Perceived Turbulence by an Aircraft

While derived gust velocity provides a measure of turbulent activity and has been used by aircraft designers for many years to characterize atmospheric turbulence, there are several problems associated with using it as a basis for an absolute turbulence scale. The problems stem from the fact that turbulent motions are sensed indirectly via the aircraft response to

atmospheric turbulence. The acceleration increment produced by a particular gust may not be the same for all airplanes. For instance, when two different–sized airplanes fly through the same turbulent region at the same speed and encounter a gust, the acceleration induced by this gust may be large in the smaller airplane and small in the larger aircraft. Also the response of an aircraft to turbulence is directly proportional to the airspeed. Doubling the airspeed will normally double the vertical acceleration increment A_n.

Since derived gust velocity is an aircraft dependent measure of turbulence intensity, its value is associated with the ability to determine how different aircraft would respond to the same gust intensity (Turner *et al.*, 1980). As a consequence of these considerations, the intensity scale based on U_{de} presented in Lee (1977) may not be applicable to all aircraft and in particular to the UND Citation.

We also note that the derived gust velocity is a measure of aircraft response to a particular turbulence eddy size (*i.e.*, 25 times the mean aerodynamic chord) whereas the total aircraft response is in fact due to the action of a range of eddy sizes as is considered in the statistical models of turbulence which led to kinetic dissipation rate.

However, we observe from Eq. (3) that kinetic dissipation rate also is an aircraft–dependent measure of turbulence because the aircraft–encountered turbulence is proportional to a number of aircraft related factors:

$$D_a^{1/2} \propto \left(\frac{C_{L_\alpha} \; S \; V_t^{4/3}}{m} \right) \epsilon^{1/3} \tag{7}$$

In fact comparing Eqs. (3) and (7), one concludes that both measures of aircraft turbulence have the *same* dependence on lift curve slope, wind area and mass. The difference in velocity dependence (U_{de} is proportional to V, whereas ϵ_a is proportional to $V^{4/3}$) probably will not be significant for aircraft of a given class in a given flight regime.

If we assume the aircraft is in level flight, then $[(C_{L_\alpha} \; S \; V_t)/m \; g]$ is constant for all aircraft. In such a case, the normalized aircraft acceleration (in units of g) is identical for all aircraft in response to a given derived gust velocity whereas $D_a^{1/2}$ will be proportional to $V_t^{1/3}$. We conclude that the use of kinetic dissipation rate to characterize the turbulence environment encountered by an aircraft in level flight will introduce a relatively weak velocity dependence which does not arise with the use of equivalent gust velocity.

2.4 Aircraft Data Overview and Selected Results

During the summer of 1983, the UND Citation II aircraft conducted flights associated with eleven storms. The storm characteristics and pilot's observations are briefly described in Table 2. The storms were of light to moderate intensity. No severe thunderstorms were encountered. Table 3 presents an overview of all the flight segments for which useful data were acquired. The altitudes of the segments and the maximum and minimum ranges associated with each flight are listed. While most of the flights took place at altitudes near 10,000 feet there are several data sets from lower and higher altitudes. Of particular importance is the range of the aircraft from the radar. Table 3 indicates that most of the flights were at ranges greater than 60 km from the radar.

Table 2. Storm Characteristics

DATE	PURPOSE	PILOT'S OBSERVATIONS	WEATHER CONDITIONS
6/14/83	Mid level turbulence	Several cloud (turret) penetrations at 11,12, 17 and 19 kft. Light turbulence observed on most penetrations. Deep haze layer & cirrus from system to west.	A high pressure system at 500 mb was rather stationary over Eastern and Northeastern U.S. sea breeze was observed. First convective cell broke out in VT about noon. During afternoon, all cells moved slowly southward.
6/15/83	Mid–upper level turbulence	Found 700–800 FPM updrafts and 600–700 FPM downdraft, airspeed fluctuations of 5–8 kts in towering cumulus (mid level 8–17 kft) alongside a line region of 40 dBZ. Finished in upper region (anvil) at 34 kft. Moderate turbulence observed in several areas, otherwise it was light.	Weather conditions were similar to the pattern on 14 June 1983. During afternoon, thunderstorms developed in central MA.
7/9/83	Mid–low level turbulence & LLWAS	Mid level (17 kft) study of light to moderate turbulecne in stratiform cloud with embedded showers. Finished with low level approaches to Hanscom through remains of a line feature. Turbulence more evident during first part of flight	The 500 mb charts had a trough positioned over New England. A cold front advanced from the west. This front produced a line of showers as it went through the area.
7/15/83	High–mid level turbulence	Sounding and measurements in thin cirrus bands (possibly anvil) at 31 kft. Larger storm system to the west did not enter study area. Also, flew at 12 kft. Occasional light turbulence on this day.	Hot and hunid with scattered cumulus.
7/21/83	High–mid level turbulence	Flew several legs at 27 kft in cirrus between larger echos. Light turbulence encountered in several areas. Lots of static caused radio and computer failures	A stronger frontal zone approached from northwest. Stronger thunderstorms developed by late afternoon. Hail reported.
8/5/83	Low level turbulence	Flew around a small (40 dBZ) cell. In haze. Occasional cumulus. Most of the flight at 5 kft.	Very warm and humid with some isolated convective clouds.

Table 2 continued

DATE	PURPOSE	PILOT'S OBSERVATIONS	WEATHER CONDITIONS
8/6/83	LLWS & High level turbulence	Flew around cells at 27 and 35 kft. Moderate turbulence.	Scattered convective activity.
8/12/83	Mid level turbulence	Boxes around area of 30 dBZ echo at several altitudes. No cumulonimbus, but moderate turbulence.	A surface low pressure moved across the southern part of New England during the day. Northeasterly winds, cool temperature (~ 50 °F) and rain was predominant throughout the day.
8/12/83	Low level wind shear & turbulence	Flew missed approaches to Hanscom and shuttled between Hanscom and Gardner at 5 kft and below.	

Table 3. Flight Data Base Overview

DATE	TIME (GMT)		FLIGHT ALTITUDE	RANGE (KM)	
	Start	End	(ft x 1000)	Minimum	Maximum
6/14/83	21:20	21:45	10	35	65
	21:55	22:05	20	35	80
6/15/83	18:10	18:46	12	60	85
	18:50	19:22	8.5	70	90
	19:27	20:11	16	70	115
	20:22	20:34	30	65	90
7/9/83	11:47	12:02	9	60	80
7/15/83	21:38	22:09	10	40	85
7/21/83	21:24	21:52	25	50	110
8/5/83	20:29	21:16	5	45	75
8/6/83	20:56	21:46	25	15	75
8/12/83	15:10	15:22	10	00	78
	15:30	16:00	4	60	100
	16:08	16:15	20	65	95
	16:37	16:44	11	70	85
	20:45	21:03	3.5	45	90

To avoid aircraft acceleration effects in the data which occur during a change of flight altitude, the data analysis focused on constant altitude segments. Figure 1 shows the time history of the aircraft altitude for the entire flight of the 15 June mission. In this case four legs of data were selected for detailed analysis.

The time series of turbulence severity index $\epsilon^{1/3}$, calculated from pressure fluctuations [Eq. (2)] and acceleration fluctuations [Eq. (3)] for the first segment of the 15 June flight are shown in Figure 2. Most of the segment took place in light turbulence while stronger turbulence was encountered towards the end of the segment. The pilots perception of encountered turbulence is indicated in Fig. 2a. Both curves show that in the region of stronger turbulence, the turbulence is not continuous but is spatially patchy or intermittent. Note that the acceleration-based estimates show better quantitative agreement with the pressure-based estimates when the turbulence is more intense.

To further quantify the degree of correlation between the pressure-based estimates $\epsilon_p^{1/3}$, and the acceleration-based estimates, $\epsilon_a^{1/3}$, a bivariate frequency distribution was developed. Table 4 indicates several suggested turbulence intensity scales. Turbulence class intervals are defined for various ranges of dissipation rate in Table 5. Tables 6 and 7 show the unnormalized and normalized bivariate frequency distribution respectively for the 15 June case. The unnormalized table is presented to give a sense of the amount of data associated with each cell pair. From Table 7, it is seen that 43.3% of the data points lie below the dashed diagonal line, a line which indicates perfect correlation between $\epsilon_p^{1/3}$ and $\epsilon_a^{1/3}$. This implies that for this case 43.3% of the aircraft measurements indicate that $\epsilon_p^{1/3} > \epsilon_a^{1/3}$ (i.e., $\epsilon_p^{1/3}$ yields stronger turbulence intensity than does $\epsilon_a^{1/3}$, 3.4% of the data shows $\epsilon_a^{1/3} > \epsilon_p^{1/3}$, and 53.3% of the data predict the same degree of turbulence severity.

An inspection of the distribution shown in Table 7 and in other tables included in Volume II indicates that in general, these two parameters ($\epsilon_p^{1/3}$ and $\epsilon_a^{1/3}$) correlate reasonably well but with a majority of data indicating $\epsilon_p^{1/3} > \epsilon_a^{1/3}$ for low level turbulence. Table 8 characterizes estimated turbulence intensities in terms of the MacCready intensity scale of Table 5.

At this point, it should be pointed out that the above statistical analysis only describes how these two parameters are jointly distributed and their class correlations. But nothing has been said about the absolute accuracy of these two parameters in measuring the turbulence intensity encountered by the airplane. Comparison of the aircraft-derived quantities $\epsilon_p^{1/3}$ and $\epsilon_a^{1/3}$ with pilot reports can be used to provide at least a qualitative check on the encountered turbulence. Thus, whenever the pilot reports of turbulence encountering were available, the descriptive magnitude of turbulence intensity and the approximate time of turbulence occurrences are indicated on the plot of $\epsilon_p^{1/3}$. Examination of the flight data clearly indicates that for the flights conducted in the summer of 1983, most flights encountered only "light" and/or "moderate" turbulence and none encountered turbulence which could be designated as "heavy".

Referring to Tables 9 and 10, which summarize the results given in Volume II, we see that $\epsilon_p^{1/3}$ usually overestimates the magnitude of turbulence intensity when compared with the pilot's description of the observed turbulence intensity. For example on June 15 (run 3),
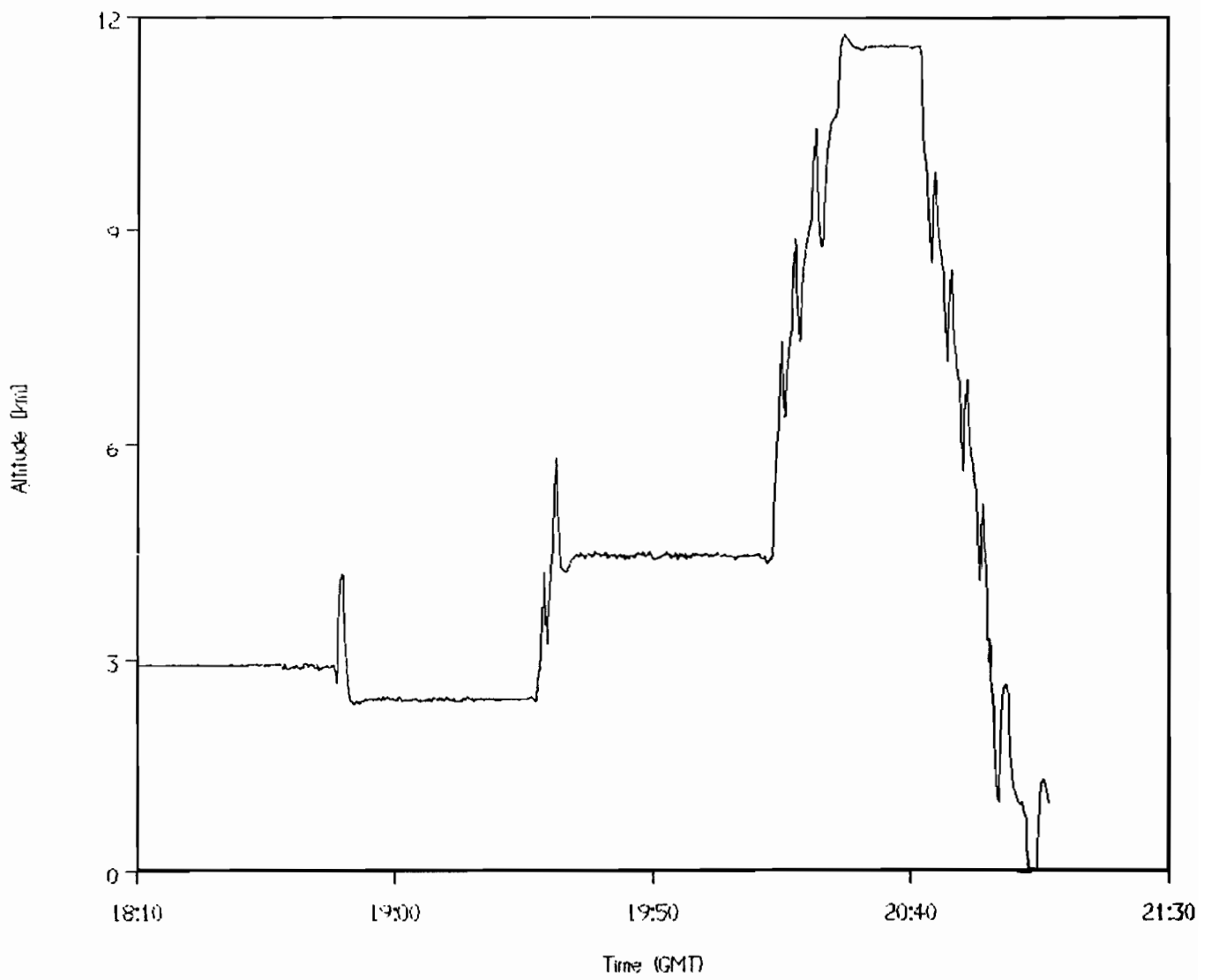
Figure 1.   Altitudes of 15 June 1983 Flight.
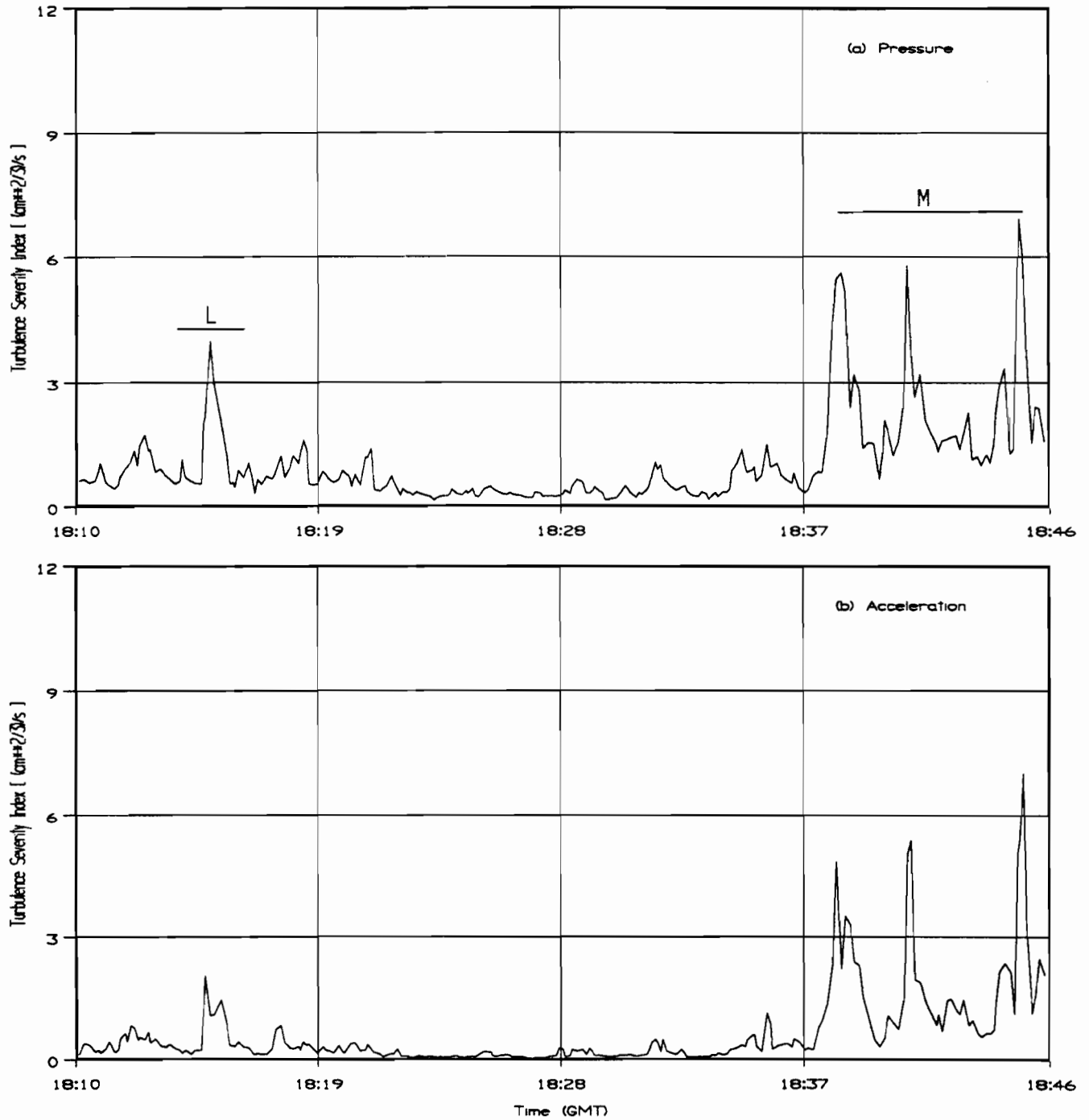
Figure 2. Time series of turbulence severity index as computed from (a) aircraft-pressure structure function and (b) aircraft-acceleration structure function for 1810 GMT to 1846 GMT 15 June 1983. Time segments during which the Citation pilot reported light (L) or moderate (M) turbulence are indicated. The altitude of the aircraft is 3.7 km.

Table 4. Turbulence Intensity Scales

$\epsilon^{1/3}$		U_{de} [*]	Turbulence Classification
MacCready	Bohne		
$0.0 < \epsilon^{1/3} < 1.5$	$0.0 < \epsilon^{1/3} < 4.0$	$3.0 < U_{de} < 6.0$	Light
$1.5 < \epsilon^{1/3} < 3.5$	$4.0 < \epsilon^{1/3} < 8.0$	$6.1 < U_{de} < 9.1$	Moderate
$3.5 < \epsilon^{1/3} < 8.2$	$8.0 < \epsilon^{1/3} < 13.0$	$9.2 < U_{de} < 12.1$	Heavy
$\epsilon^{1/3} > 8.2$	$\epsilon^{1/3} > 13.0$	$U_{de} > 12.2$	Extreme

$\epsilon^{1/3}$ = Turbulence severity index ($cm^{2/3}$/sec)

U_{de} = Derived gust velocity (m/sec)

---

[*] Presented by Lee (1977).

Class	Interval
1	$0.0 < TSI < 0.6$
2	$0.6 < TSI < 1.2$
3	$1.2 < TSI < 1.8$
4	$1.8 < TSI < 2.4$
5	$2.4 < TSI < 3.0$
6	$3.0 < TSI < 3.6$
7	$3.6 < TSI < 4.2$
8	$4.2 < TSI < 4.8$
9	$4.8 < TSI < 5.4$
10	$5.4 < TSI < 6.0$
11	$6.0 < TSI < 6.6$
12	$6.6 < TSI < 7.2$
13	$7.2 < TSI < 7.8$
14	$7.8 < TSI < 8.4$
15	$8.4 < TSI$

Table 5: Turbulence severity index (TSI in $cm^{2/3}sec^{-1}$) intervals used in subsequent bivariate frequency analyses

Date: 6-15-83   Time: 1810 GMT to 1846 GMT

ACCELERATION	1	2	3	4	5	6	7	8	9	10	11	12	13
15									1				
14													
13													
12													
11								1	1				
10													
9					1			1	2		1	2	
8					1						1		
7										1			
6				1	1	1		1					
5			1	2	1	2	2	1	1				
4		1	1	3	4	2	3		1	1	1		
3		3	11	10	1	2		2					
2	23	30	13	6	1	2							
1	249	122	23	5									

PRESSURE

Table 6: Bivariate frequency distribution of turbulence severity index computed from aircraft-acceleration structure function, $\epsilon_a^{1/3}$ (ordinate) and aircraft-pressure structure function, $\epsilon_p^{1/3}$ (abscissa) for 1810 GMT to 1846 GMT 15 June 1983. The total number of occurrences is 545. The aircraft altitude is 3.7 km.

Date: 6-15-83   Time: 1810 GMT to 1846 GMT

ACCELERATION	1	2	3	4	5	6	7	8	9	10	11	12	13
15									.002				
14													
13													
12													
11								.002	.002				
10													
9					.002			.002	.004		.002	.004	
8					.002						.002		
7										.002			
6				.002	.002	.002		.002					
5			.002	.004	.002	.004	.004	.002	.002				
4		.002	.002	.006	.007	.004	.006		.002	.002	.002		
3		.006	.020	.018	.002	.004		.004					
2	.042	.055	.024	.006	.002	.004							
1	.457	.224	.042	.009									
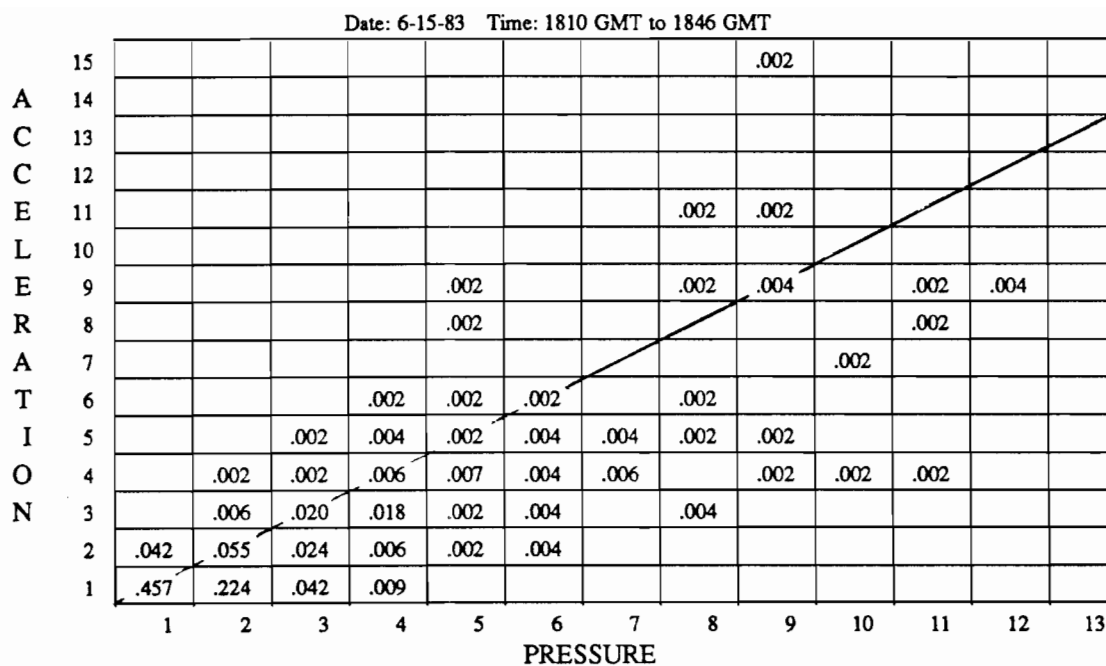
PRESSURE

Table 7: Normalized bivariate frequency distribution of turbulence severity index computed from aircraft-acceleration structure function $\epsilon_a^{1/3}$ (ordinate) and aircraft-pressure structure function, $\epsilon_p^{1/3}$ (abscissa) for 1810 GMT to 1846 GMT 15 June 1983. Total number of occurrences is 545. To calculate the number of occurrences for each cell, multiply the nomalized cell frequency by the total number of occurrences. The diagonal line indicates perfect correlation between $\epsilon_a^{1/3}$ and $\epsilon_p^{1/3}$.

Date: 6-15-83   Time: 1810 GMT to 1846 GMT

MacCready Intensity Scale		Normalized Frequency Distribution	
Class	Interval	Pressure	Acceleration
Negligible	0.0 < TSI < 0.6	0.457	0.732
Light	0.6 < TSI < 1.5	0.350	0.171
Moderate	1.5 < TSI < 3.5	0.139	0.070
Heavy	3.5 < TSI < 8.2	0.053	0.026
Extreme	8.2 < TSI	0.000	0.002

Table 8:   Normalized frequency distribution of aircraft–based turbulence severity index computed from aircraft–pressure structure function and aircraft–acceleration structure function relative to the MacCready Turbulence Intensity Scale for 1810 GMT to 1846 GMT 15 June 1983. The total number of occurrences is 545. To calculate the number of occurrences for each category,   multiply the nomalized frequency by the total number of occurrences.

Table 9. Frequency of occurrence of $\epsilon_p^{1/3}$ corresponding to MacCready Turbulence Intensity Scale for the data inferred from aircraft measurements. Refer to Table 4 for appropriate intensity classifications.

RUN NO.	DATE	TIME (GMT) Start	End	MACCREADY TURBULENCE INTENSITY SCALE Negligible	Light	Moderate	Heavy	Extreme	Total
1	6/14/83	21:20	21:45	0.227	0.556	0.211	0.005		1.0
2		21:55	22:05	0.464	0.503	0.033			1.0
3	6/15/83	18:10	18:46	0.457	0.350	0.139	0.053		1.0
4		18:50	19:22	0.151	0.504	0.306	0.039		1.0
5		19:27	20:11	0.236	0.456	0.226	0.078	0.005	1.0
6		20:22	20:34	0.122	0.403	0.436	0.039		1.0
7	7/9/83	11:47	12:02	0.185	0.700	0.115			1.0
8	7/15/83	21:38	22:09	0.510	0.390	0.098	0.002		1.0
9	7/21/83	21:25	21:52	0.406	0.518	0.076	0.009		1.0
10	8/5/83	20:29	21:16	0.456	0.443	0.092	0.009		1.0
11	8/6/83	20:56	21:46	0.262	0.634	0.103	0.001		1.0
12	8/12/83	15:10	15:22	0.277	0.514	0.254	0.006		1.0
13		15:30	16:00	0.416	0.531	0.053			1.0
14		16:08	16:15	0.114	0.505	0.276	0.105		1.0
15		16:37	16:44	0.029	0.495	0.457	0.019		1.0
16		20:45	21:03	0.125	0.593	0.260	0.022		1.0

Table 10. Frequency of occurrence of $\epsilon_a^{1/3}$ corresponding to MacCready Turbulence Intensity Scale for the data inferred from aircraft measurements. Refer to Table 4 for appropriate intensity classifications.

RUN NO.	DATE	TIME (GMT) Start	End	MACCREADY TURBULENCE INTENSITY SCALE Negligible	Light	Moderate	Heavy	Extreme	Total
1	6/14/83	21:20	21:45	0.690	0.307	0.003			1.0
2		21:55	22:05	0.921	0.079				1.0
3	6/15/83	18:10	18:46	0.732	0.171	0.070	0.026	0.002	1.0
4		18:50	19:22	0.541	0.324	0.122	0.012		1.0
5		19:27	20:11	0.408	0.383	0.155	0.054		1.0
6		20:22	20:34	0.177	0.481	0.331	0.011		1.0
7	7/9/83	11:47	12:02	0.789	0.207	0.004			1.0
8	7/15/83	21:38	22:09	0.844	0.149	0.006			1.0
9	7/21/83	21:25	21:52	0.587	0.279	0.125	0.010		1.0
10	8/5/83	20:29	21:16	0.910	0.080	0.010			1.0
11	8/6/83	20:56	21:46	0.897	0.067	0.030	0.005		1.0
12	8/12/83	15:10	15:22	0.785	0.188	0.028			1.0
13		15:30	16:00	0.969	0.031				1.0
14		16:08	16:15	0.733	0.190	0.076			1.0
15		16:37	16:44	0.657	0.305	0.038			1.0
16		20:45	21:03	0.674	0.304	0.022			1.0

of the 36 minutes of flight data, 35% of the data were computed as "light" turbulence, 13.9% as "moderate" turbulence, and 5.3% as "heavy" turbulence.

To examine how well the parameter U_{de} predicts turbulence intensity, the time series of U_{de} computed from Eq. (5) is plotted in Figure 3 along with pilot reports on turbulence severity. The corresponding time series of the absolute instantaneous vertical acceleration is also plotted for reference in Figure 3. The temporal variations in U_{de} and vertical acceleration are similar to the patterns of $\epsilon_p^{1/3}$ and $\epsilon_a^{1/3}$ (Figure 2). But a close examination of those figures reveals that the turbulence intensity scales inferred from the different schemes are significantly different. For example, over the time interval 1837 GMT to 1846 GMT 15 June 1983 shown in Figure 2, the peak values of $\epsilon_p^{1/3}$ and $\epsilon_a^{1/3}$ approximately indicate a "heavy" to "extreme" turbulence, according to the U_{de} intensity scale (see Figure 3 and Table 5). The peak acceleration U_{de}= 5.6 m/sec was $D_g = 0.7$. This is the highest gust-induced vertical acceleration increment observed for all the flights. A value of $D_g = 0.7$ corresponds to moderate turbulence which matches the air crew's reported turbulence as "light to moderate". On this particular segment of flight, U_{de} matched pilot reports better than $\epsilon_a^{1/3}$ and $\epsilon_p^{1/3}$. Inspection of other time histories of U_{de} indicates that the turbulence intensity inferred from the U_{de} scale occasionally matches the pilot's description of the turbulence level, but overall U_{de} suggested a significantly lower turbulence level than was reported by the pilot.

2.5 Discussion of Aircraft Turbulence Intensity Scale

Using inertial subrange concepts, the turbulence kinetic energy dissipation rate ϵ can be related to the velocity structure function. Associated with the structure function is a dimensionless constant C [see Eqs. (2) and (3)] which is very important in determining the magnitude of ϵ. Unfortunately, a wide range exists in the published values of the constant C. Differences by a factor of two or even more are common because of different ways the velocity spectrum can be normalized and the definition of the spectral density. Table 11 lists the values of C found so far in the literature. Various values have been used for the constant C in Kolmogorov's formula (structure function), possibly because of estimating different meteorological parameters (i.e., momentum flux, heat flux, or moisture flux, etc.) from the data taken from the surface layer either over water or over land under different atmospheric stability conditions (i.e., neutral, stable or unstable). To our best understanding, none of the values of C listed in Table 11 were determined from experimental data taken directly from a meteorological situation similar to those which we consider in this report. It has been pointed out that the exact value of C cannot be considered completely established and further investigation is needed (MacCready, 1964; Champagne et al., 1977).

The impact of this variability need not be significant in the context of NEXRAD as long as all the processors use the same constant. Of greater importance is the fact that the MacCready intensity scale, which was based on a limited number of stiff winged aircraft structures generally assigns ϵ values to intensity classes higher than is actually experienced by the Citation. Thus the MacCready scale shown in Table 4 may be inappropriate as a hazard threshold for many modern aircraft.
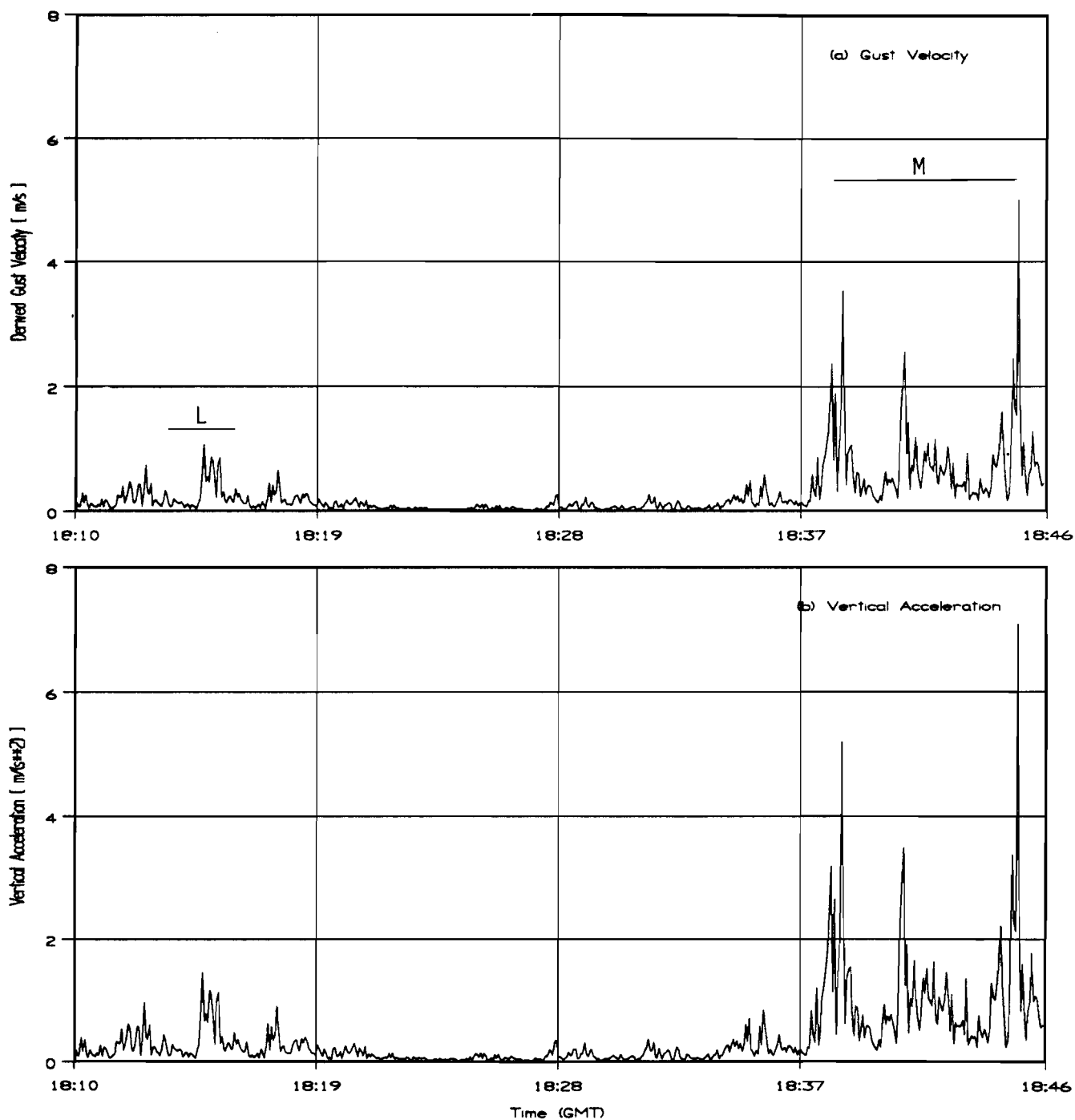
Figure 3. Time series of (a) derived gust velocity computed from the aircraft-measure vertical acceleration and (b) aircraft-measured vertical acceleration for 1810 GMT to 1846 GMT 15 June 1983. Time segments during which the Citation pilot reported light (L) or moderate (M) turbulence are indicated. The altitude of the aircraft is 3.7 km.

- 23 -

Table 11. Constant C in Kolmogorov's Structure Function

Author	
	1.77 to 0.8
Obukhov & Yaglom (1951)	1.6
Takeuchi (1962)	1.3 (surface boundary layer)
Frisch & Clifford (1974)	1.4 (longitudinal)
Cadet (1977)	1.64 (longitudinal) 2.19 (transverse) 3.83 (2-dimensional spectra; clear air turbulence in stratosphere)
Gage (1979)	2.33 (longitudinal) 2.91 (transverse)
Labitt (1981)	1.77 (longitudinal)
Bohne (1982), after Panchev (1971)	1.35 (water turbulence in tidal channel)
Gossard et al. (1984)	2.0 to 2.2 (clear air turbulence)

2.6 Summary of Section 2

Results of the statistical analyses of the numerical values of $\epsilon_p^{1/3}$ and $\epsilon_a^{1/3}$ for the 494 minutes of useful aircraft data indicate that the agreement is reasonably good for a majority of the data. Comparisons of the intensity scales inferred from $\epsilon_p^{1/3}$ or $\epsilon_a^{1/3}$ with the pilot indications of turbulence intensity effectively demonstrate that $\epsilon_a^{1/3}$ using MacCready's scales overestimate the severity of turbulence as reported by the pilot. As can be seen from Table 3, the flight altitudes varied from 3,500 ft to 30,000 ft for the missions conducted in 1983. There is no obvious relationship between flight altitude and the correlation between $\epsilon_a^{1/3}$ and $\epsilon_p^{1/3}$.

The magnitude of turbulence intensity scales inferred from $\epsilon^{1/3}$ and U_{de} were found to be inconsistent for the data analyzed. Occasionally, the pilot's description of aircraft response approximately matched the turbulence intensity level inferred from U_{de} scale. In general, the U_{de} scales underestimated the magnitude of turbulence intensity as reported by the pilot.

3. KINETIC ENERGY DISSIPATION RATE ESTIMATION FROM DOPPLER WEATHER RADAR DATA

Estimation of storm turbulence using Doppler weather radar spectra has been accomplished by Frisch and Clifford (1974), Frisch and Strauch (1976), Lee (1972), Labitt (1981) and Bohne (1982). The intensity of turbulence is inferred from analysis of the Doppler spectrum. In particular, the spectrum width provides a useful signature of turbulent activity in the atmosphere. Labitt (1981) has shown that the Doppler spectrum width can be related to the turbulent kinetic energy dissipation rate ϵ by the relationship:

$$\epsilon_r^{1/3} = \frac{C_F \, \sigma_\nu}{1.35 \, a^{1/3}} \quad cm^{2/3} sec^{-1} \tag{8}$$

where

$\quad$ CF $\quad$ = Conversion factor

$\quad \sigma_\nu \quad$ = spectrum width (m/sec)

$\quad$ a $\quad$ = radar two-way half-Gaussian beamwidth (km)

$$= \frac{R\theta}{(8 \ln 4)^{1/2}}$$

$\quad$ R $\quad$ = range (km)

$\quad \theta \quad$ = one-way half power beamwidth (radians)

The principal assumptions made in deriving Eq. (8) are:

(1) the turbulence is homogeneous and isotropic,

(2) the radar senses only turbulence in the inertial subrange, thus turbulence is characterized by the spatial energy density spectrum given by Kolmogorov's law:

$$E(K) = C \, \epsilon^{2/3} K^{-5/3} \tag{9}$$

$\quad$ with K the wavenumber, C Kolmogorov's constant, and

(3) the radar resolution cell extent is smaller than the resolution cell cross range extent.

Bohne (1982) defined a more refined model that considers the imperfect response of raindrops to the wind field and the effect of turbulence outer scale in the relationship between spectrum width and $\epsilon^{1/3}$. Bohne's refinements have been incorporated in the NEXRAD JSPO (1985) limited production turbulence detection algorithm.

We remark that assumptions (1) and (2) imply an upper bound on the detection range of the algorithm in that the size of the radar resolution cell must be smaller than the size of the largest turbulent eddy in the inertial subrange, known as the turbulence outer scale. Since

the size of the radar resolution cell increases with range it is clear that for a given turbulence outer scale there exists a range beyond which the resolution cell contains scales outside the inertial subrange. Unfortunately, the actual turbulence outer scale defining the boundary of the inertial subrange varies spatially with storm intensity and structure values from 300 m to several kilometers have been reported in the literature. Bohne (1982) suggests 2 km as a typical value for a convective storm. Thus when observing less intense storms at long range it is very probable that the resolution cell size exceeds the turbulence outer scale and the radar is sensing non-homogeneous turbulence which cannot be quantitatively characterized using the inertial subrange concept. Under such conditions the radar still provides a measure of turbulent activity but its interpretation is not clear.

3.1 Data and Method of Analysis

The Doppler weather radar spectrum width data used in this study were obtained from an S-band pencil beam radar operated by the Massachusetts Institute of Technology (MIT). The characteristics of the radar are listed in Table 12.

The 3 dB beamwidth of the MIT S-band weather radar is 1.45 degrees, almost 50% wider than the beamwidth of the NEXRAD system. The impact of the wider beamwidth is that the results are indicative of NEXRAD radar performance at ranges scaled up by a factor of 1.45. Hence results for ranges from 70 km to 90 km would be representative of NEXRAD performance at ranges from 101 km to 130 km. Thus most of the results from the 1983 data sets reflect long range NEXRAD performance in the detection of light to moderate turbulence.

The MIT radar was operated using the random phase technique discussed by Laird (1981) to prevent out-of-trip weather from corrupting the first trip data. Clutter removal was accomplished by the mean-level subtractor technique developed by Anderson (1981). Autocorrelation values for lags 0, 1, and 2 were estimated by conventional techniques using a 96-pulse coherent processing interval (CPI). The autocorrelation lags were then converted to weather parameter moments using the equations:

Reflectivity:
$$dBz = 10 \log k \; \frac{|R_1|^{4/3}}{|R_2|^{1/3}} \tag{10}$$

Mean radial velocity:
$$v = \frac{\lambda}{4\pi T} \tan^{-1} \left[\frac{Im(R_1)}{Re(R_1)} \right] \tag{11}$$

Velocity variance:
$$\sigma_v^2 = \frac{\lambda^2}{24\pi^2 T^2} \ln \left[\frac{|R_1|}{|R_2|} \right] \tag{12}$$

Signal-to-noise ratio:
$$\frac{S}{N} = \left[\frac{R_0 R_2^{1/3}}{R_1^{4/3}} \right]^{-1} \tag{13}$$

where R_n is the nth autocorrelation lag estimate, λ is the radar wavelength, T is the interpulse period and k is a range dependent constant determined from the radar parameters and STC

Table 12. MIT Radar Characteristics

Antenna

Beamwidth	1.45° one-way
Maximum roataion rate	6 r.p.m (both axes)

Transmitter

Pulse length	1 microsecond
PRF	912 Hz
Frequency	2705 MHz
Maximum unambiguous range	164 km
Maximum unambiguous velocity	25 m/s

Receiver

Bandwidth	1.1 MHz

Digital Signal Processor

Range sample spacing	1/16, 1/8, 1/4, 1/2 nmi.
Number of range gates processed	288
Algorithm	pulse-pair processing
Processor output	0th, 1st and 2nd moments

law. Notice that Eq. (12) uses the so called lag 1-2 spectrum width estimator. This estimator was selected due to the use of the random phase technique which essentially transforms second trip weather into wideband noise making the estimation of the signal portion of S/N more difficult.

Both Labitt's formula [Eq. (8)] and the NEXRAD algorithm have been used to estimate $\epsilon^{1/3}$ from the radar data in this study. It is to be noted that neither algorithm utilizes any information regarding storm structure or features associated with convective activity.

Initial processing of the spectrum width data used a signal-to-noise ratio (SNR) of 10 dB. As will be seen in the next section, use of higher SNR levels was found to be required in order to minimize erroneous spectrum width estimates from causing false alarms in turbulence detection.

The estimated turbulence intensities obtained from Eg. (8) at each point of a radar volume scan were averaged over a three-dimensional Cartesian grid. The horizontal and vertical spacing of the grid were adjustable in the data reduction software. A higher resolution grid size (1 km x 1 km x 1 km) was selected to validate the turbulence measurements, while a lower resolution grid size provided an indicator of the performance of the NEXRAD-layered turbulence product, as defined in the NEXRAD Technical Requirements (NTR) (NEXRAD JSPO, 1985).

More specifically, the FAA has requested maps depicting hazardous weather layered to match the altitude sectors used by enroute controllers. Typical current values for these sectors are:

(1) low altitude: surface to 24 kft,

(2) high altitude: 24 kft to 33 kft, and

(3) superhigh altitude: above 33 kft.

Accordingly, the current NEXRAD JSPO (1985) specification calls for averaging the radar turbulence estimates $\epsilon_r^{1/3}$ horizontally and vertically to form layers which correspond to the altitudes identified above with a 4 km x 4 km horizontal resolution. To minimize the effect of ground clutter on the weather parameter estimates, we have changed the lowest section to include altitudes from approximately 1 kft to 24 kft. Various grid systems are used for the analysis of each selected data set. The scales used in this report are listed in Table 13.

It is assumed that turbulence is the primary contributor to Doppler spectrum variance. Other factors, such as wind shear and distribution of fall velocities of the raindrops, also contribute to spectral broadening but are considered negligible. In a later section we will comment further on these factors.

Since the final turbulence product is an average over the volume defined by the layer dimensions rather than a point value, we have also averaged the point values of each individual aircraft derived quantity ($\epsilon_p^{1/3}$, $\epsilon_a^{1/3}$, and U_{de}) within the corresponding layer volumes so that comparisons of aircraft and radar data are made on the basis of average value. Some comparisons of peak aircraft $\epsilon_p^{1/3}$ and $\epsilon_a^{1/3}$ with an average radar $\epsilon_r^{1/3}$ were also made.

Table 13. Scales Used in the Analysis of the Layered Radar Quantities

CASE	RESOLUTION (KM)		RESOLUTION (KM)	REMARKS
	Δx	Δy	Δz	
I[1]	1	1	1[2]	Basic scale used for comparing aircraft data with radar data
II	4	4	1[2]	Evaluating horizontal differences due to the change in horizontal scale as compared with Case I
IIIa	1	1	0.3 – 7.3	Evaluating vertical differences
IIIb	1	1	7.3 – 10.0	due to the change in vertical scale as
IIIc	1	1	above 10.0	compared with Case I
IVa	4	4	0.3 – 7.3	Evaluating both vertical and
IVb	4	4	7.3 – 10.0	horizontal differences
IVc	4	4	above 10.0	

[1] This case is analogous to the "point by point" comparisons used by Labitt (1981) and Bohne (1982) in which the weather radar tracked the aircraft.

[2] The vertical resolution Δz = 1 km is the layer thickness, which is centered on the actual aircraft flight height.

Employing Eq. (8) the radar spectrum width data were used to estimate the turbulence intensity $\epsilon_r^{1/3}$ comparable to the aircraft derived quantities $\epsilon_p^{1/3}$, $\epsilon_a^{1/3}$ or U_{de}. Since the radar operated in a volume scan mode (*i.e.*, a sequence of sector scans at different elevation angles), as opposed to an aircraft tracking mode, the following technique was used to develop a time series of $\epsilon_r^{1/3}$ along the aircraft track. Aircraft position information, obtained from Air Traffic Control Radar Beacon System (ATCRBS) beacon reports and from the aircraft inertial navigation system was used to identify radar observations associated with a particular layered volume with corresponding aircraft observations made during passage through the volume. By repeating the correlation process for temporally coincident radar and aircraft observations, a time series of radar measurements along the aircraft track can be formed which exhibits gaps corresponding to times when the radar was not observing the aircraft location. Such time series plots have been developed for radar reflectivity, spectrum width, and kinetic energy dissipation rate. While minor data alignment problems exist due to slight timing and aircraft position errors, they are not considered significant in view of the spatial layer grid size.

Bivariate frequency distributions were also developed for the pairs [$\epsilon_r^{1/3}$, $\epsilon_p^{1/3}$] and [$\epsilon_r^{1/3}$, $\epsilon_a^{1/3}$]. For convenience, the gaps in the time series of $\epsilon_r^{1/3}$ were arbitrarily mapped into radar turbulence class 1 in the frequency distribution. Thus meaningful information regarding radar/aircraft data comparisons is associated with radar turbulence classes 2 through 15.

3.2 Comparison of Aircraft and Radar Data

In this section we present typical examples of aircraft/radar turbulence data comparisons. First we consider the radar data corresponding to the aircraft data in Figure 2. Figure 4 shows the radar reflectivity, spectrum width, and turbulence severity index ($\epsilon^{1/3}$) computed for a sequence of 1 km x 1 km x 1 km layers along the aircraft track developed using the temporal/positional correlation technique discussed above. The turbulence severity indices were estimated using Labitt's algorithm [Eq. (8)]. Several points are to be noted. The gaps in the time series correspond to times during which the aircraft was not scanned by the radar. Figure 4b indicates the narrowest spectrum widths occurring at times earlier than 1837 GMT, with several missing widths noted. These additional gaps in the spectrum width field are due to invalid estimates associated with noisy correlation lag estimates (*i.e.*, negative widths were computed). The remaining spectrum widths map into the indicated turbulence severity indices. Figure 4c is to be compared with Figure 2a. In both cases the strongest turbulence levels occur after 1837 GMT. The highest reflectivity between 1819 GMT and 1828 GMT is associated with a very narrow width and a corresponding low turbulence level that correlates well with the aircraft data. However, the other spectrum widths occurring before 1837 GMT map into turbulence levels higher than indicated in the aircraft data.

The narrowness of the widths and the fact that they are associated with lower reflectivity levels suggests that the width estimates themselves may be noisy enough to account for the overestimation of the turbulence intensity by the radar. This is corroborated by Table 4 showing the corresponding bivariate class distribution of the radar and aircraft data. Table 14 indicates a large variability in the radar data associated with the lowest class in the aircraft data. Most of the encountered turbulence was relatively light.

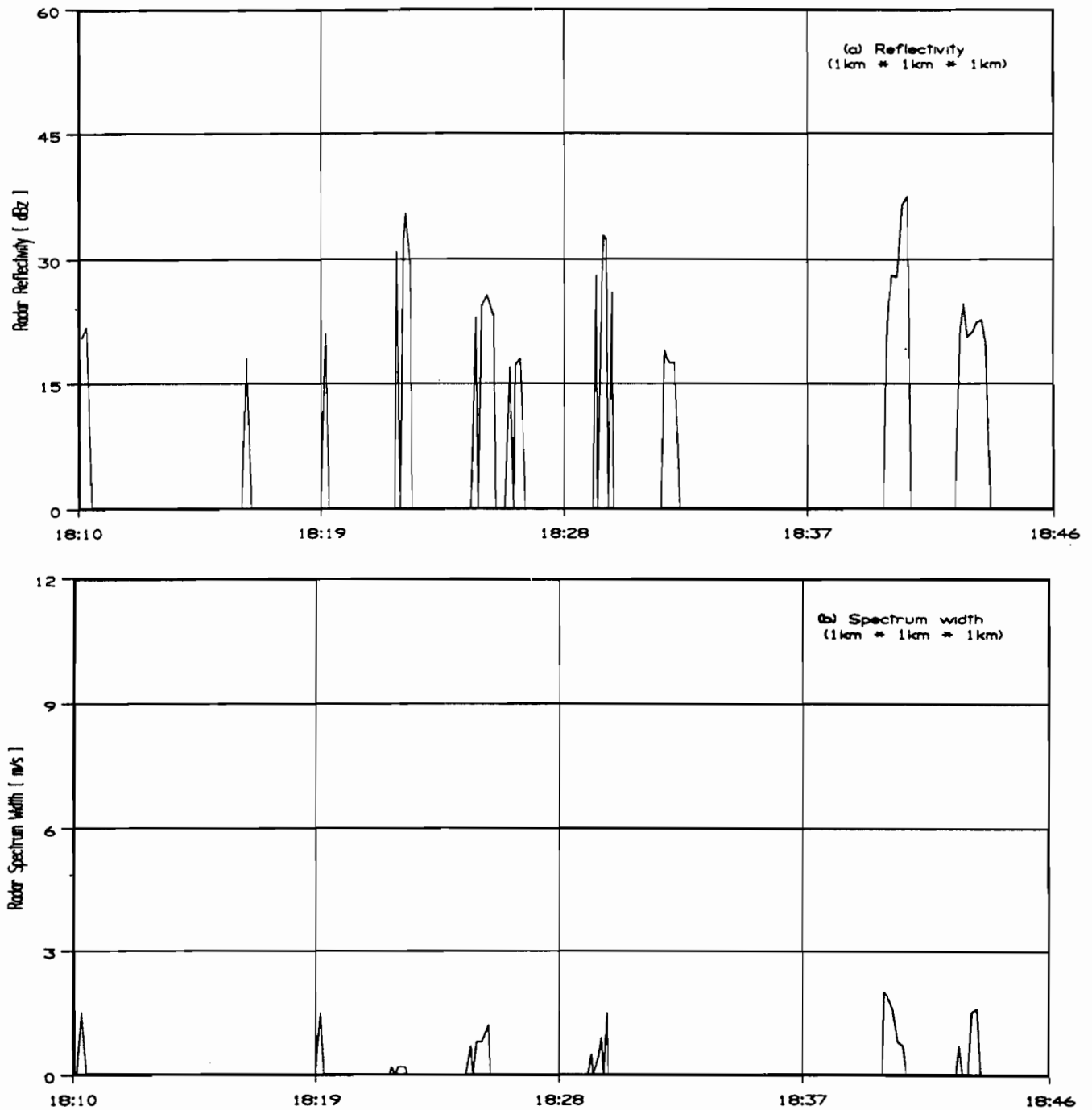Figure 4. Time series of (a) layered radar reflectivity, (b) layered radar spectrum width and (c) turbulence severity index computed from the layered radar spectrum width along the aircraft track for 1810 GMT to 1846 GMT 15 June 1983. The dimensions of the layers are 1 km x 1 km x 1 km centered on the aircraft. The altitude of the aircraft is 3.7 km.
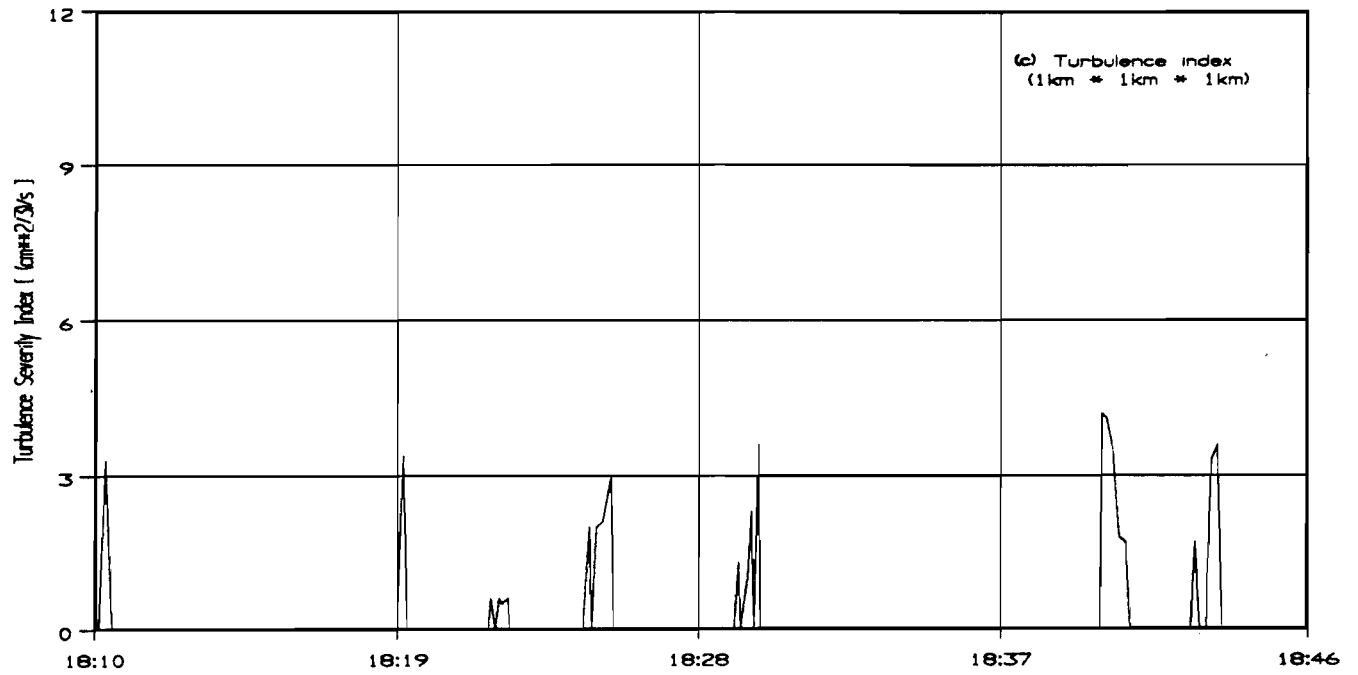
Mission Date: 6/15/83

Figure 4 continued.

RADAR	1	2	3	4	5	6	7	8	9	10	11	12	13
15													
14													
13													
12													
11													
10													
9													
8													
7			.004	.004									
6	.004	.016	.004										
5	.004												
4	.016												
3	.004		.008		.004								
2	.004												
1	.426	.261	.133	.036	.016	.012	.012	.004	.004	.016	.004	.004	

AIRCRAFT PRESSURE

Table 14: Normalized bivariate frequency distribution of turbulence severity index computed from layered spectrum width, $\epsilon_r^{1/3}$ and aircraft–pressure structure function, $\epsilon_p^{1/3}$ for 1810 GMT to 1846 GMT 15 June 1983.

Figure 5 shows aircraft-based turbulence estimates for a larger portion of the same flight. The altitude was 5.3 km and the range varied from about 95 km at time 1927 GMT to 65 km at time 1948 GMT to 115 km at time 2008 GMT. As before, the aircraft data indicate both the intermittent nature of the encountered turbulence and good correlation between the pressure and acceleration based estimates for stronger turbulence levels. The corresponding radar data are presented in Figure 6 and Table 15. We see that the radar overestimates turbulence severity, as compared to the aircraft estimates. The results were also noted by Bohne (1985). Low level turbulence is associated with the greatest radar measurement variability. Comparing Figure 6c with Figure 5a we see that the radar estimates do tend to track the pattern of increases and decreases exhibited by the aircraft turbulence estimates. The radar estimates always exhibit broader peaks not only due to the volume filtering inherent in the radar measurements but primarily due to the smoothing effects of the layering process.

The data in Table 15 have been recast in Figure 7 in terms of the probability of equaling or exceeding a given level of turbulence. The rate of decrease in the probabilities as a function of severity class is very similar for the aircraft and radar data. However, the radar estimates clearly provided a generally higher level of turbulence than was measured aboard the aircraft.

As a further example of the effects of layering we present Figure 8, which shows the result of horizontal layering, vertical layering and combined horizontal/vertical layering, for comparison with the data presented in Figure 6c. Horizontal layering, as mentioned earlier, involves a grid spacing of 4 km while the vertical layering extends from an altitude of 0.3 km to 7.3 km, corresponding to the lowest enroute altitude sector of interest. The horizontal layering always tends to broaden the stronger turbulence regions. Depending on the homogeneity of the turbulence environment, layering causes variations in the turbulence values. Vertical layering resulted only in minor changes in the turbulence intensities. Comparing Figure 8c with Figure 5a, it is clear that the general pattern of turbulence fluctuations is still present in the layered product but regions of light turbulence are much less clearly defined.

In order to investigate the performance of the turbulence algorithm for higher levels of turbulence, Tables 16, 17, 18 and 19 are presented. These tables present the normalized bivariate frequency distribution of turbulence severity index computed from the various combinations of layered (1 km x 1 km x 1 km and 4 km x 4 km x (0.3 to 7.3) km) radar spectrum width and aircraft-based measurements. The data from all 1983 flights were combined to produce these tables. It is apparent that for both layered products, the radar overestimates turbulence severity index when compared to aircraft-based estimates. Bohne (1985) also observed this characteristic of the algorithm.

3.3 Turbulence Outer Scale

The NEXRAD JSPO (1985) turbulence algorithm (developed by Bohne 1982) incorporates two effects neglected in Labitt's (1981) formulation. The primary refinement involves the effect of a finite turbulence outer scale. Labitt made an infinite turbulence outer scale assumption primarily for reasons of mathematical tractability. Bohne's formulation was more realistic but required numerical techniques for its development. As turbulence outer scale decreases, estimates derived from Bohne's algorithm deviate more and more from
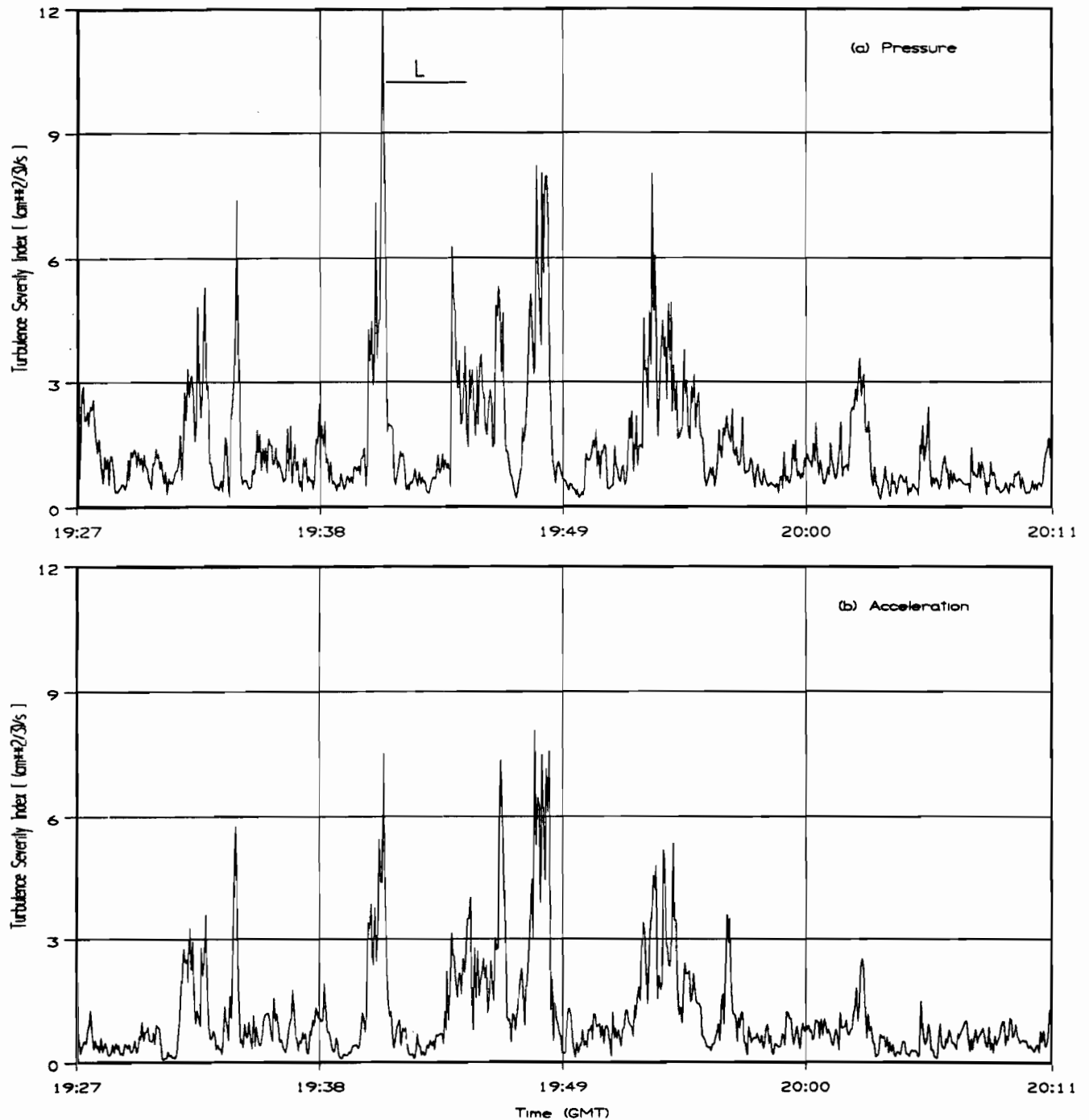
Figure 5. Time series of turbulence severity index as computed from (a) aircraft–pressure structure function and (b) aircraft–acceleration structure function for 1927 GMT to 2011 GMT 15 June 1983. The time segment during which the Citation pilot indicated light (L) turbulence is indicated. The altitude of the aircraft is 5.3 km.
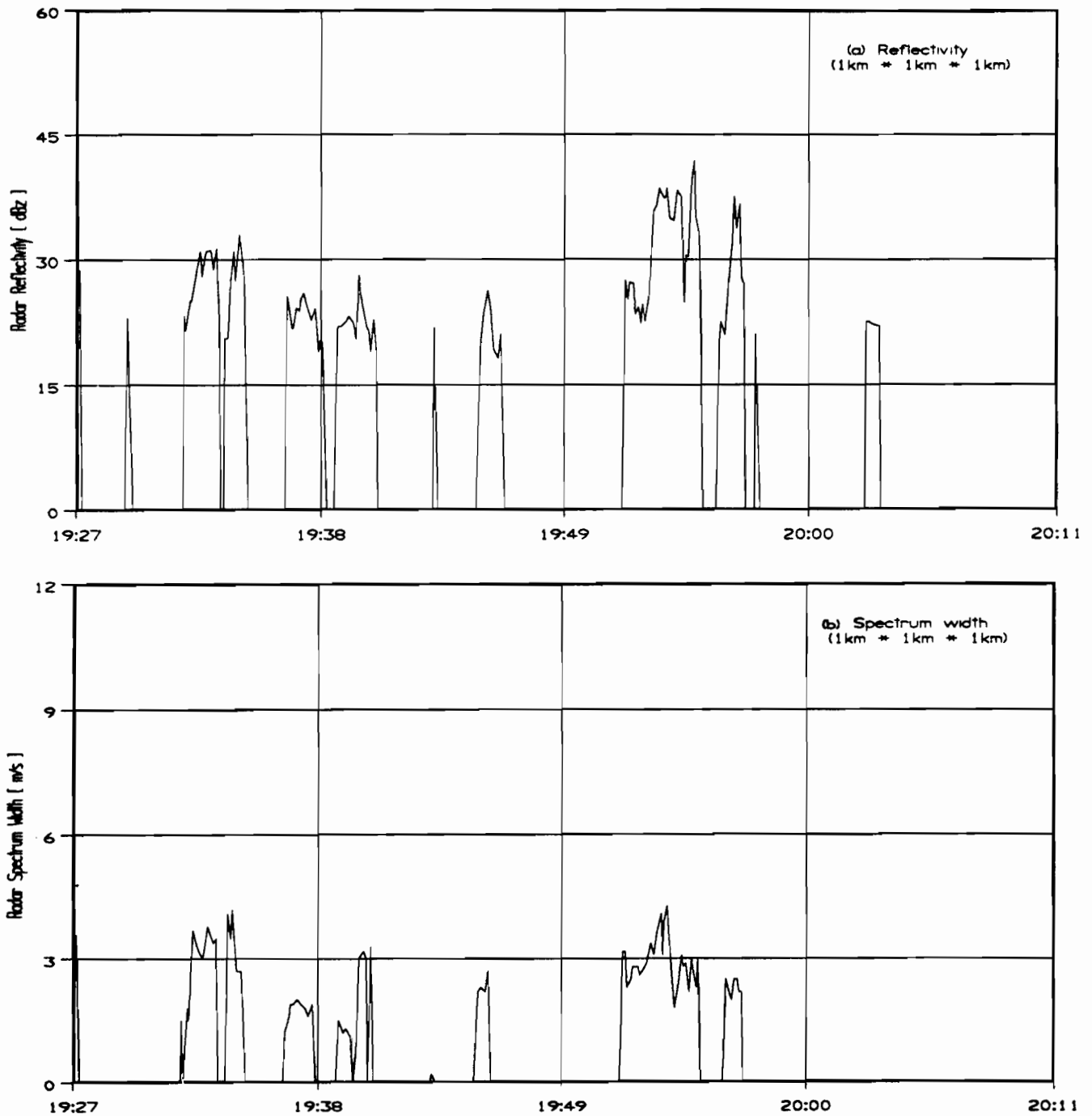
Figure 6.   Time series of (a) layered radar reflectivity, (b) layered radar spectrum width and (c) turbulence severity index computed from the layered radar spectrum width along the aircraft track for 1927 GMT to 2011 GMT 15 June 1983. The dimensions of the layers are 1 km x 1 km x 1 km centered on the aircraft. The altitude of the aircraft is 5.3 km.
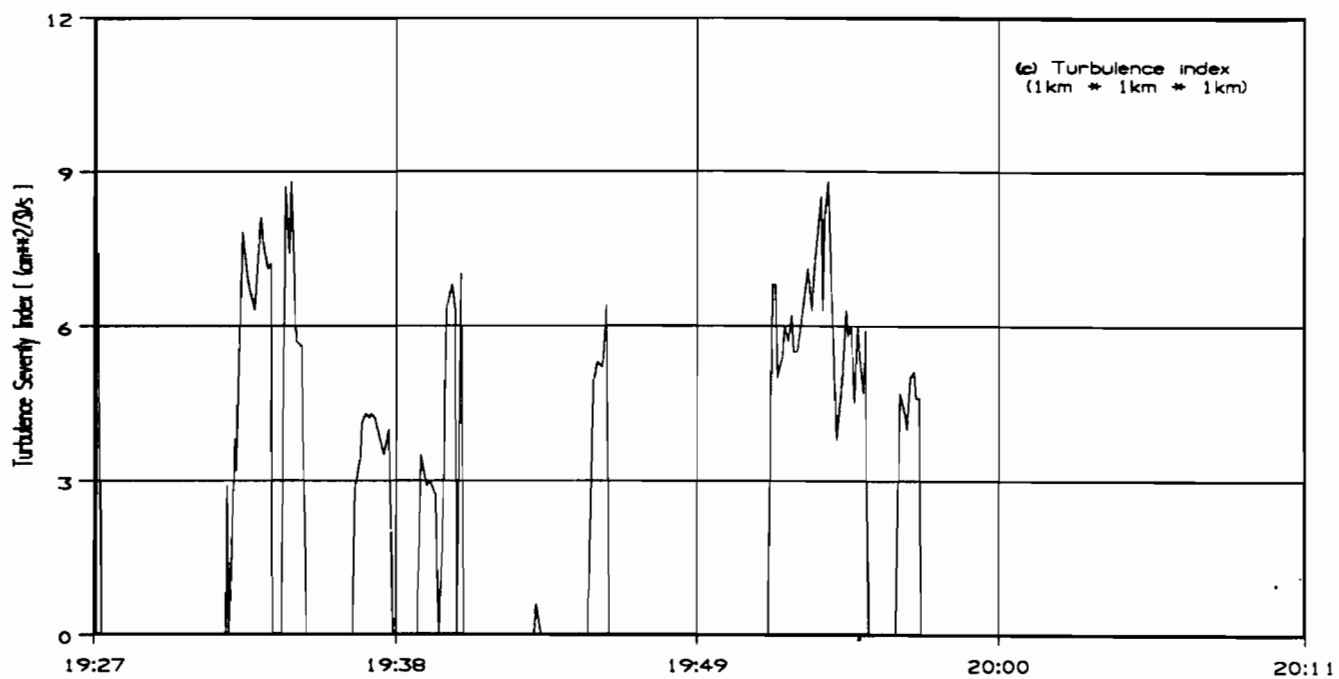
Mission Date: 6/15/83

(c) Turbulence index
(1km * 1km * 1km)

Figure 6 continued.

RADAR	1	2	3	4	5	6	7	8	9	10	11	12	13	14	15
15		.003					.009								
14			.003				.003								
13		.006		.006	.003										
12	.009	.006			.003	.003	.003		.003						
11		.003	.003	.003	.006	.003	.003	.003	.003						
10		.006	.006		.012	.006	.003								
9		.003	.006	.009	.003	.006									
8		.006	.012	.006											
7	.003	.012		.003	.003	.003									
6		.009				.003									
5	.003	.006		.003	.003										
4															
3		.003													
2															
1	.178	.371	.087	.040	.022	.025	.009	.003	.009	.009		.003		.006	.003

AIRCRAFT PRESSURE

Table 15: Normalized bivariate frequency distribution of turbulence severity index computed from layered spectrum width, $\epsilon_r^{1/3}$ and aircraft–pressure structure function, $\epsilon_p^{1/3}$ for 1927 GMT to 2011 GMT 15 June 1983.
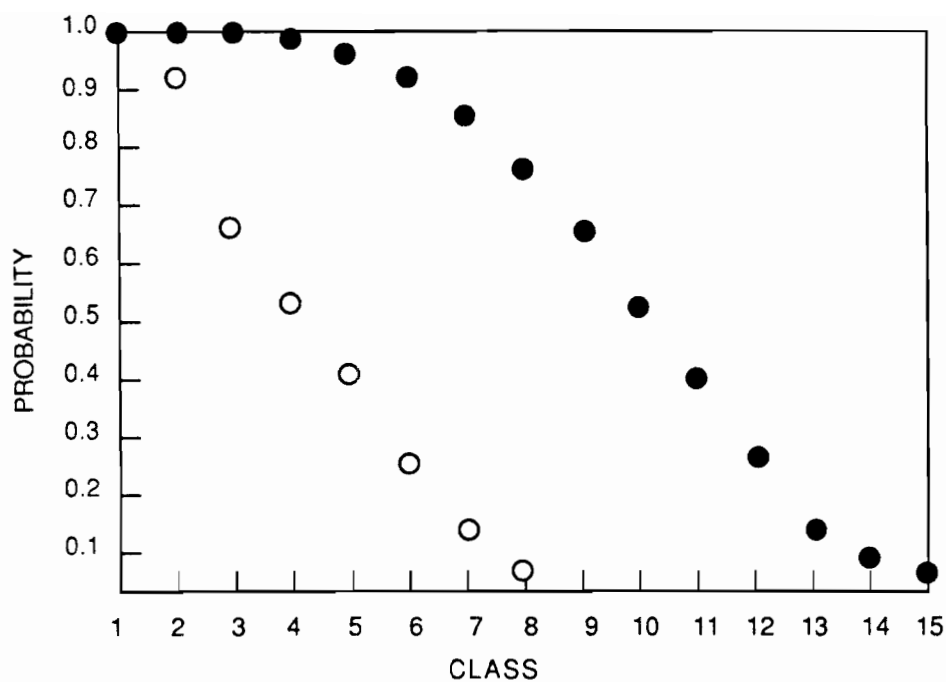
Figure 7. Probability that the turbulence severity index, computed from aircraft–pressure structure function (open circles) and from layered radar spectrum width (closed circles), equals or exceeds a specified category of turbulence severity index. The data used to generate this graph were taken from Table 15. The categories are described in Table 6.
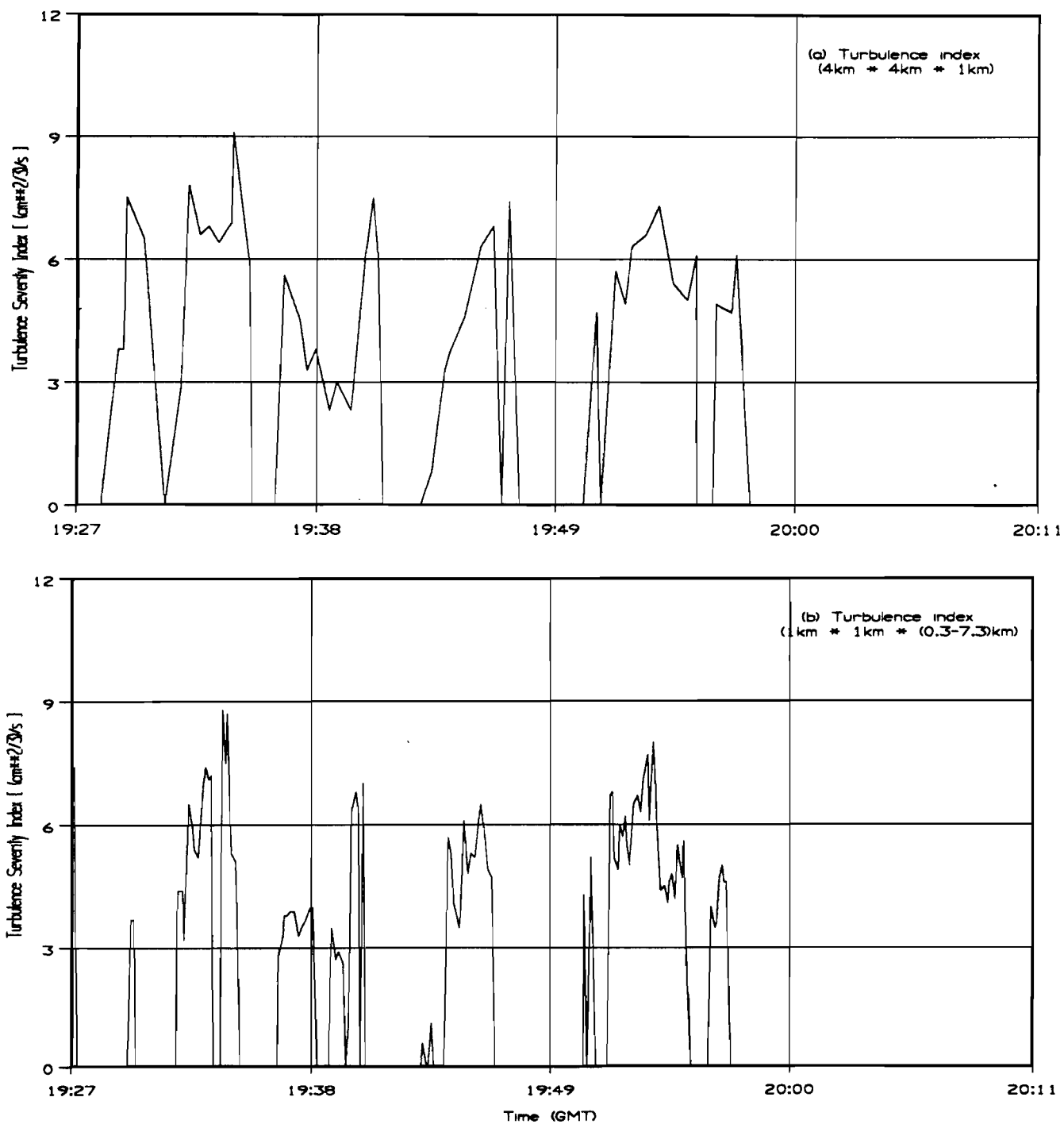
Figure 8. Time series of turbulence severity index computed from layered radar spectrum width along the aircraft track for 1927 GMT to 2011 GMT 15 June 1983. The dimensions of the layers (x, y, z) are (a) 4 km x 4 km x 1 km centered on the aircraft, (b) 1 km x 1 km x (0.3 to 7.3) km above the ground and (c) 4 km x 4 km x (0.7 to 7.3) km above the ground. The altitude of the aircraft is 5.3 km.
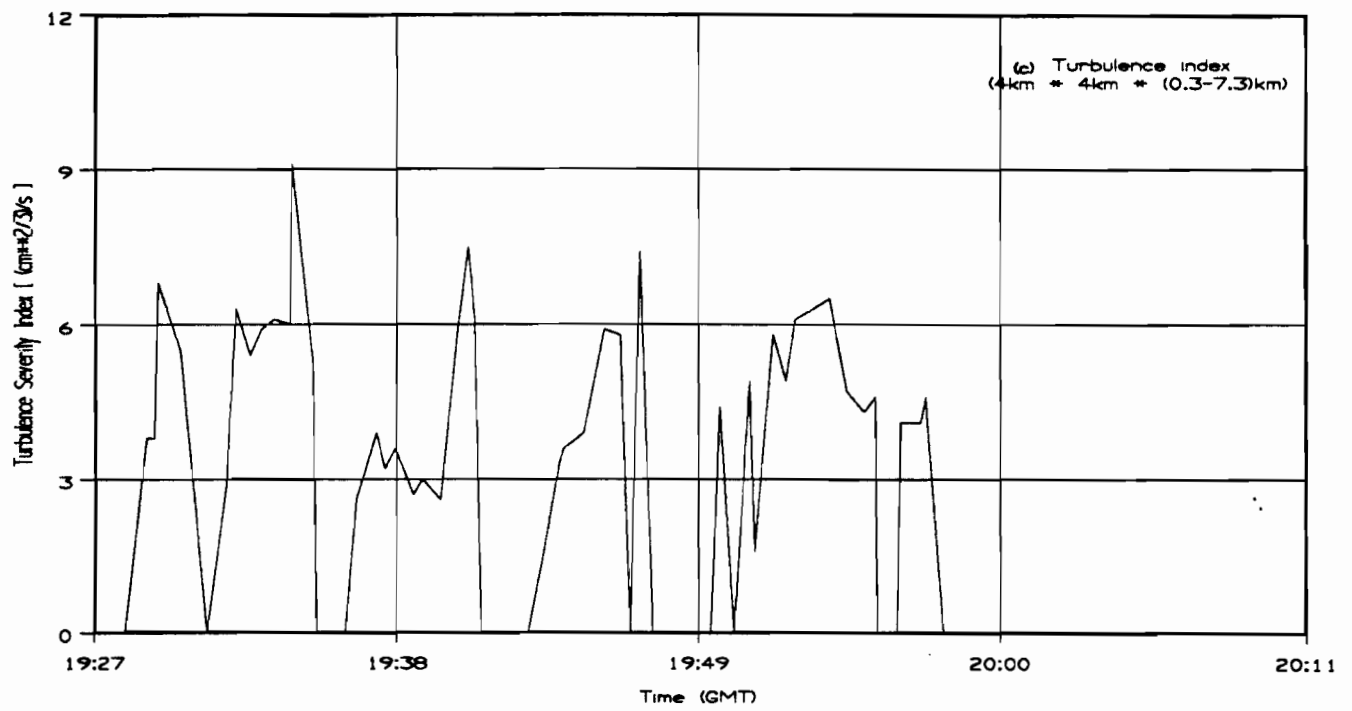
Figure 8 continued.

RADAR	3	4	5	6	7	8	9	10	11	12	13
15	.016			.008	.023						
14	.016	.008			.008						
13		.016	.008								
12		.008	.008	.008	.008		.008				
11	.039	.023	.016	.008	.008	.008	.008				
10	.047	.008	.047	.023	.008				.008		
9	.055	.047	.008	.016	.008	.008					
8	.078	.023	.008						.008		
7	.039	.023	.023	.008		.008					
6	.117	.016	.008	.008							
5	.031	.008	.016								
4	.008	.008									
3	.016		.016								

AIRCRAFT PRESSURE

Table 16 : Normalized bivariate frequency distribution of turbulence severity index computed from layered spectrum width, $\epsilon_r^{1/3}$ and aircraft-pressure structure function, $\epsilon_p^{1/3}$ for all flights. The layer dimensions are 1 km x 1 km x 1 km. The categories shown correspond to moderate or greater turbulence based upon the MacCready Turbulence Intensity Scale.

		3	4	5	6	7	8	9	10	11	12	13
	15	.026	.013			.013						
	14	.026	.013									
	13	.013	.026	.013		.013	.013					
	12	.039	.013	.013			.013					
R	11	.026		.026	.013	.013						.013
A	10	.079	.013	.039	.026							
D	9	.053	.026	.039								
A	8	.053	.013	.026								
R	7	.079	.039	.026	.013							
	6	.013	.013	.013				.013				
	5	.013	.013	.013								
	4		.013	.026								
	3											

AIRCRAFT PRESSURE

Table 17 : Normalized bivariate frequency distribution of turbulence severity index computed from layered spectrum width, $\epsilon_r^{1/3}$ and aircraft–pressure structure function, $\epsilon_p^{1/3}$ for all flights. The layer dimensions are 4 km x 4 km x (0.3 to 7.3) km. The categories shown correspond to moderate or greater turbulence based upon the MacCready Turbulence Intensity Scale.

RADAR	3	4	5	6	7	8	9	10	11	12	13
15		.015	.015				.015				
14						.015					
13	.015	.015		.015							
12			.015	.029							
11	.044	.029	.015			.015	.015				
10	.132	.029	.015	.015	.015	.015					
9	.044	.088	.015								
8	.088	.015		.105							
7	.059	.015	.015			.015					
6	.044	.029									
5	.015		.029								
4											
3	.015	.015									

AIRCRAFT ACCELERATION

Table 18 : Normalized bivariate frequency distribution of turbulence severity index computed from layered spectrum width, $\epsilon_r^{1/3}$ and aircraft-pressure structure function, $\epsilon_a^{1/3}$ for all flights. The layer dimensions are 1 km x 1 km x 1 km. The categories shown correspond to moderate or greater turbulence based upon the MacCready Turbulence Intensity Scale.

RADAR		3	4	5	6	7	8	9	10	11	12	13
R	15	.043	.022	.022	.022			.022				
	14											
	13	.043		.022	.022							
	12	.043	.022	.022								
R	11	.022		.022	.043		.022					
A	10	.043	.043	.022	.022							
D	9	.022	.065									
A	8		.022	.022								
R	7	.087	.022			.043						
	6	.043	.022	.022								
	5	.043										
	4	.022	.022									
	3											

AIRCRAFT ACCELERATION

Table 19: Normalized bivariate frequency distribution of turbulence severity index computed from layered spectrum width, $\epsilon_r^{1/3}$ and aircraft-pressure structure function, $\epsilon_a^{1/3}$ for all flights. The layer dimensions are 4 km x 4 km x (0.3 to 7.3) km. The categories shown correspond to moderate or greater turbulence based upon the MacCready Turbulence Intensity Scale.

estimates based on Labitt's algorithm. Bohne's estimates always exceed Labitt's estimates. The second refinement due to Bohne is the effect of imperfect precipitation particle response to the wind field. This effect is significant only for ranges less than about 20 km and for cases where the turbulence outer scale is less than 0.5 km.

For illustrative purposes, Figures 9 and 10 show plots of $\epsilon_r^{1/3}$ estimates for turbulence outer scales of 0.5 km, 1.0 km, 2.0 km and 3.0 km. Figure 9 is based on a 1 km x 1 km x 1 km layer size while Figure 10 corresponds to a 4 km x 4 km x (0.3 – 7.3) km layer. While gross turbulence fluctuation patterns are retained the radar overestimation is more exaggerated for the NEXRAD algorithm than for Labitt's estimates. The unrealistic assumption of infinite outer scale in Labitt's algorithm yields the best agreement with the aircraft data.

3.4 Spectral Broadening Factors

It is clear from the comparisons presented that in general the radar estimates of turbulence intensity exceeded the aircraft estimates, particularly for low levels of turbulence. In this section we discuss several factors which can contribute to broadening of the Doppler spectrum. As discussed in the literature (Doviak and Zrnic', 1984) mechanisms which cause increased spectrum width include wind shear, antenna motion, and variations in the precipitation fallspeed and turbulence. Since they are independent of each other we can express the total Doppler variance as

$$\sigma_v^2 = \sigma_s^2 + \sigma_\alpha^2 + \sigma_d^2 + \sigma_t^2 \tag{14}$$

where σ_s^2 is the shear contribution, σ_α^2 is due to antenna motion, σ_d^2 is caused by fallspeed variations, and σ_t^2 is due to turbulence.

Antenna motion and fallspeed variation contribute little to the total spectrum width. Broadening due to antenna motion is related to rotation velocity according to:

$$\sigma_\alpha^2 = (\alpha \lambda \cos \frac{\theta_e}{2\pi\theta_1})^2 \ln 2 \tag{15}$$

where α is the rotation rate, λ is the wavelength, θ_e is the elevation angle and θ_1 is the one-way 3–dB beamwidth. For the MIT radar, the rotation rate was typically 20 °/sec, yielding a σ_a of about 0.2 m/s. The fallspeed contribution is related to the spread in the terminal velocity of various size drops by:

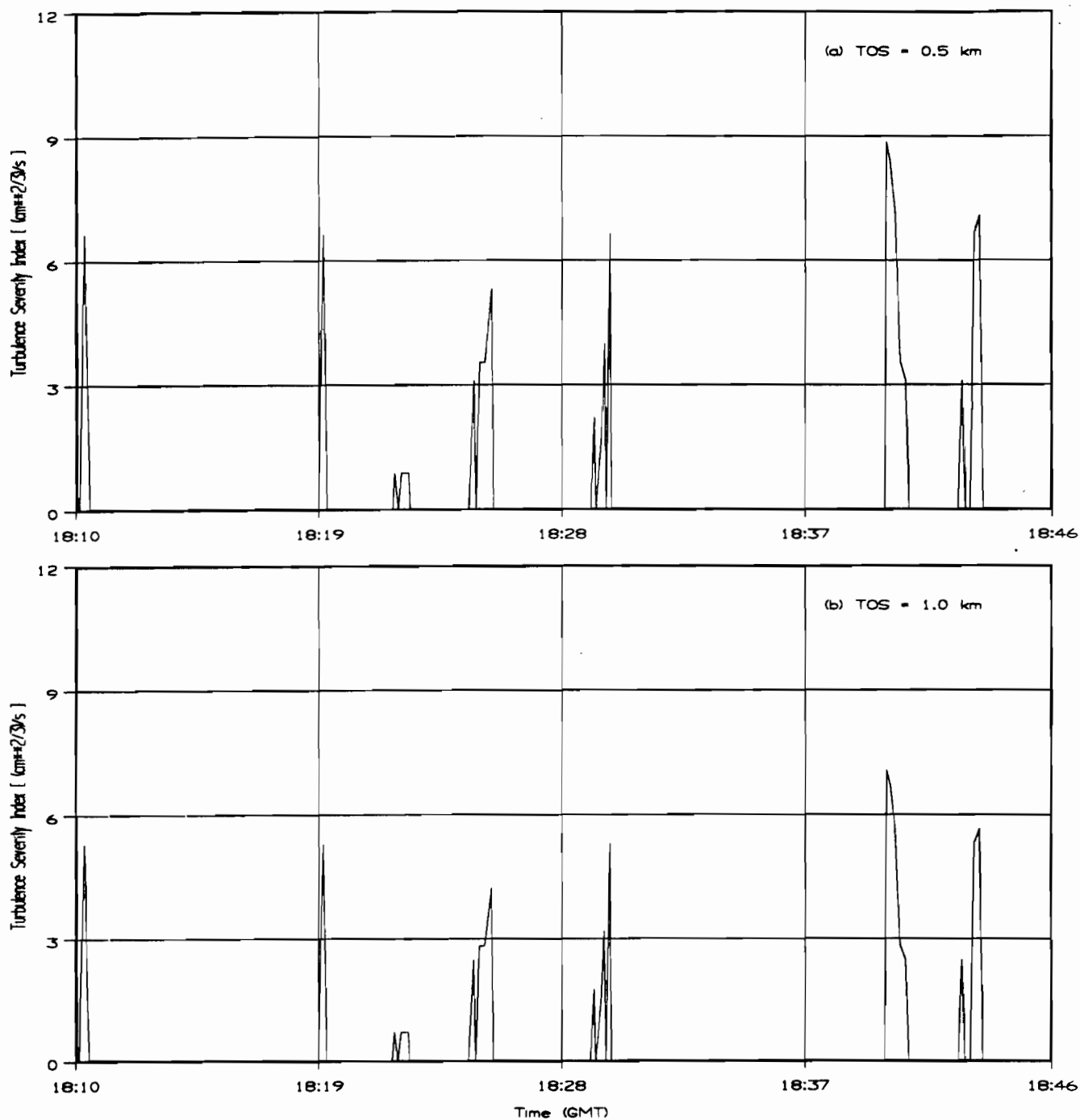$$\sigma_d^2 = (\sigma_{do} \sin \theta_e)^2 \tag{16}$$

Figure 9.   Time series of turbulence severity index computed from layered radar spectrum width for 1810 GMT to 1846 GM 15 June 1983. The dimensions of the layer are 1 km x 1 km x 1 km centered on the aircraft. The altitude of the aircraft is 5.25 km. In computing these indicies, the turbulence outer scale (TOS) was assumed to be (a) 0.5 km, (b) 1.0 km, (c) 2.0 m and (d) 3.0 km.
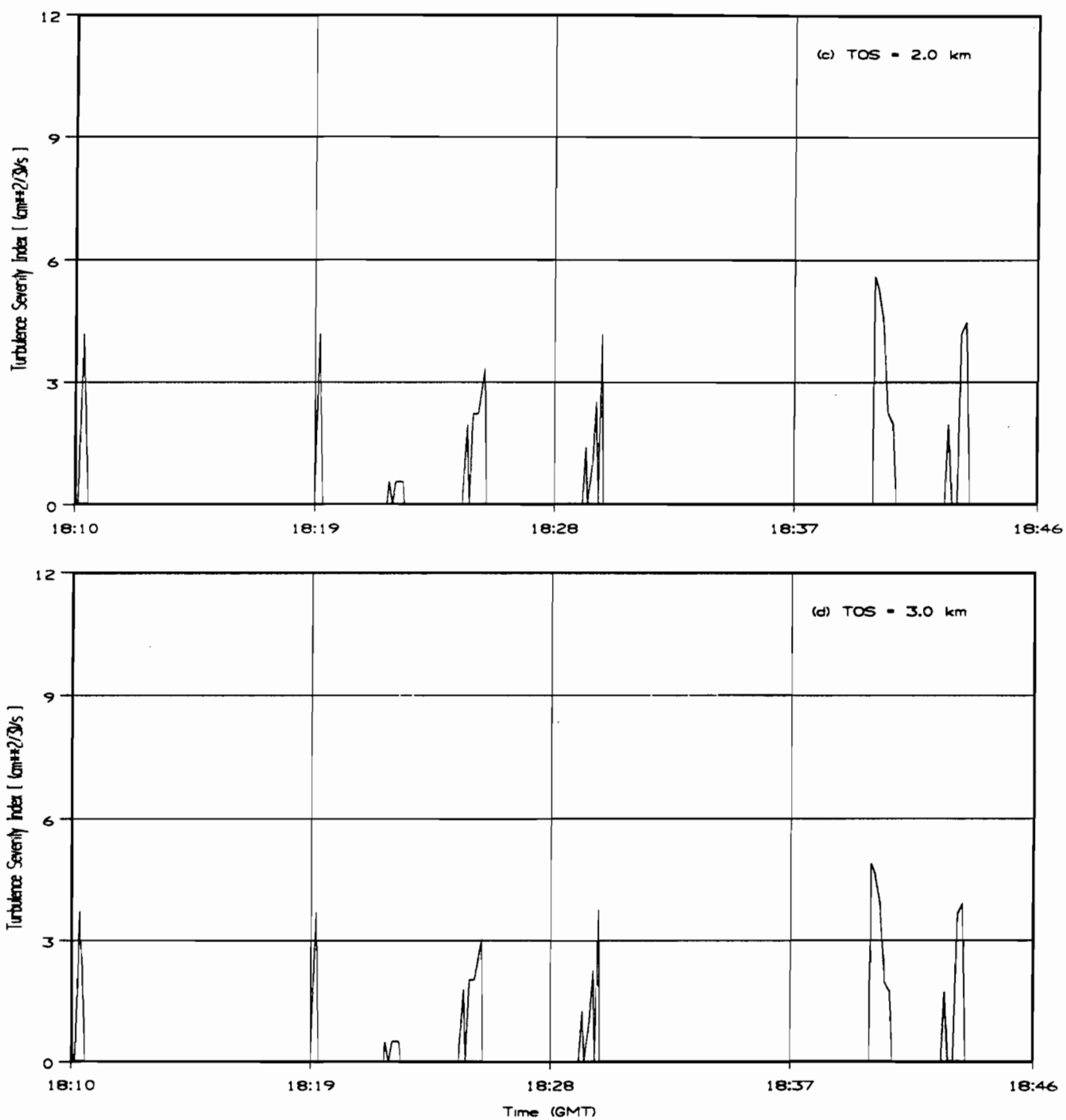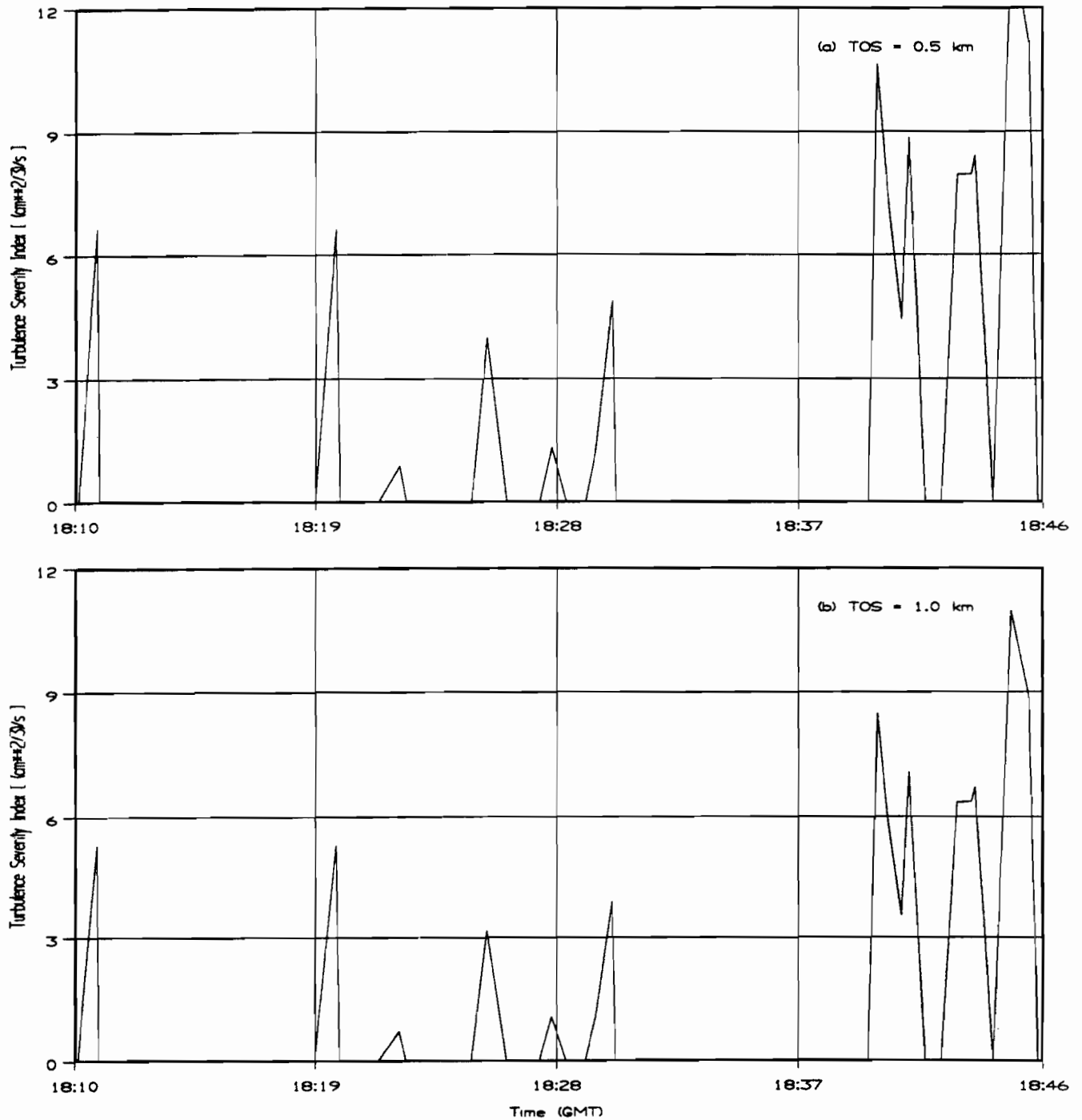
Figure 9 continued.

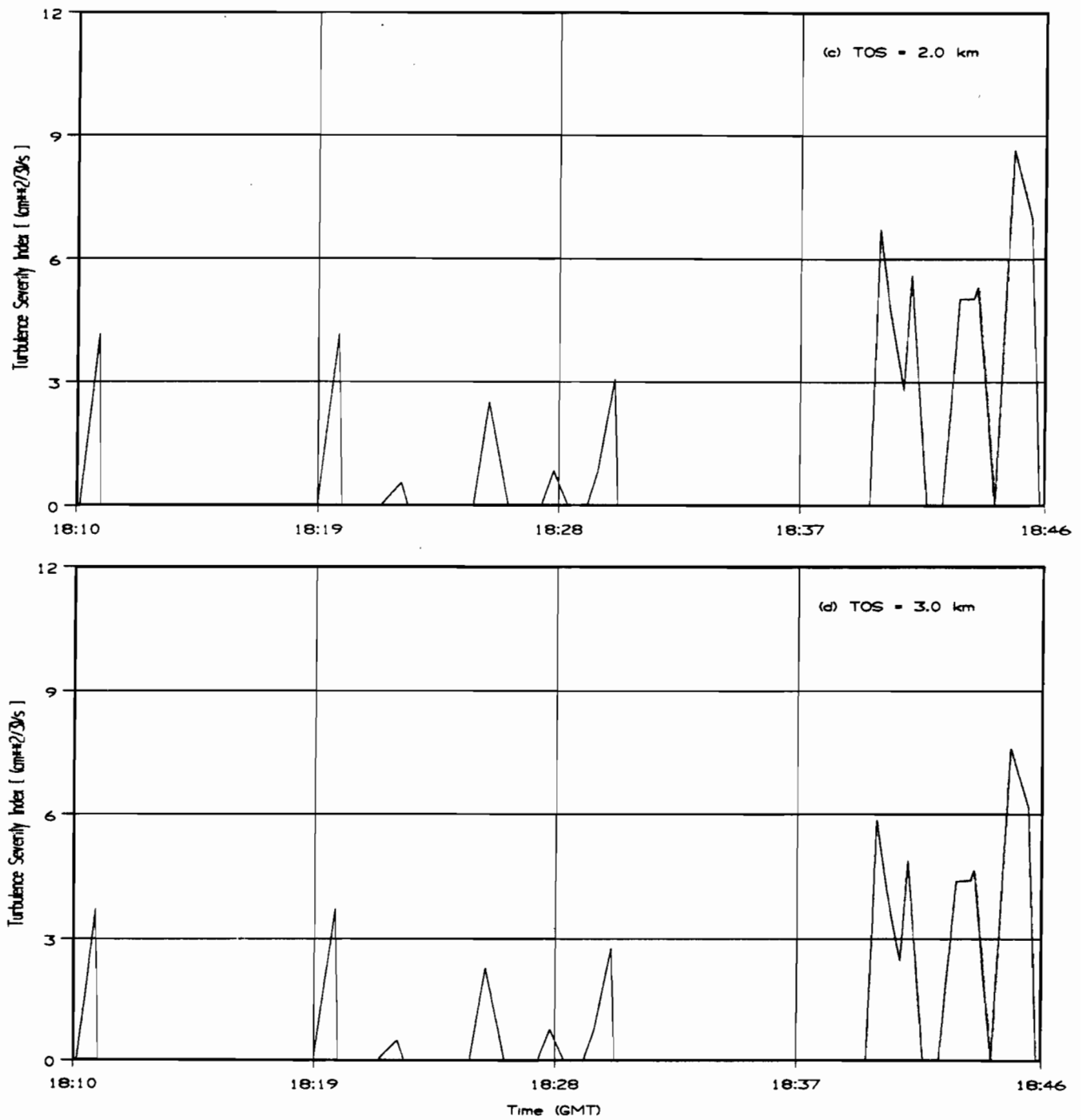Figure 10. Time series of turbulence severity index computed from layered radar spectrum width for 1810 GMT to 1846 GMT 15 June 1983. The dimensions of the layer are 4 km x 4 km x (0.3 to 7.3) km above the ground. The altitude of the aircraft is 5.25 km. In computing these indicies, the turbulence outer scale (TOS) was assumed to be (a) 0.5 km, (b) 1.0 km, (c) 2.0 km and (d) 3.0 km.

Figure 10 continued.

The width σ_{do} has been experimentally measured to be about 1 m/s so that for low elevation angles σ_d^2 becomes negligible. At a θ_e of 5°, σ_d is 0.09 m/s while at a θ_e of 10°, σ_d is 0.17 m/s.

The shear term σ_s^2 has components from angular shear in azimuth and elevation and from shear along the radial direction. Assuming linear shears and a symmetric beam pattern we have:

$$\sigma_s^2 = (R\sigma_\theta)^2 (k_\theta^2 + k_\phi^2) + (\sigma_r k_r)^2 \tag{17}$$

where k_θ, k_ϕ, and k_r are the shear coefficients in the azimuthal, elevation, and radial directions respectively. R is the range, and the terms σ_θ^2 and σ_r^2 for a circularly symmetric Gaussian antenna pattern and a Gaussian receiver response, are given by:

$$\sigma_\theta^2 = \frac{\theta_1^2}{16 \ln 2} \tag{18}$$

$$\sigma_r^2 = (0.35 \, c\tau/2) \tag{19}$$

where τ is the transmitted pulse duration. It is clear that shear effects are greater at long range and wider beamwidths.

As an example of the significance of the shear contribution, consider Figure 11 which shows the vertical profile of mean velocity and the turbulence intensity estimates associated with an RHI scan taken on August 12, 1983. The corresponding aircraft data taken within minutes of the data shown in Figure 11 indicate that the aircraft actually encountered light turbulence. Figure 11a clearly shows a vertical variation in velocity having an average shear of 4.57 x 10^{-3}/sec. Such a shear value maps into a spectrum width of 2.43 m/s and an indicated turbulence severity index of 4.78 $cm^{2/3}$ sec^{-1}, heavy turbulence according to MacCready's scale. Comparing Figure 11a with Figure 11b we see that regions of rapid vertical changes in velocity (i.e., larger gradients) correlate well with regions of strong turbulence indications. Figure 12 shows similar data corresponding to horizontal velocity gradients.

We remark that the distinction between shear and turbulence is rather vague and is primarily related to eddy size. Large shear by itself is not necessarily hazardous to aircraft, but such shears may give rise to intense turbulence. This large shear provides one indication of the likelihood of the occurrence of strong turbulence. Another interpretation of shear is that shear is an indication of the presence of turbulence contributions from scales outside the inertial subrange. Hence large shear suggests that the parametric relation between spectrum width and dissipation rate may be invalid.
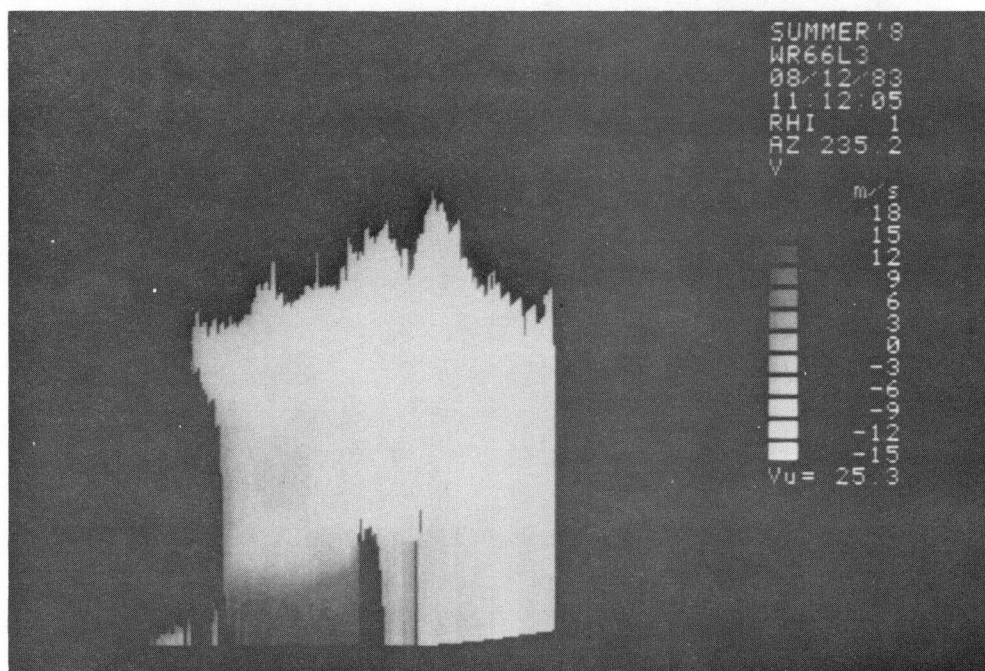
Figure 11. RHI of (a) mean Doppler velocity (V in m/s) and (b) turbulence severity index (EP in $cm^{2/3} sec^{-1}$) for 1112 GMT 12 August 1983.
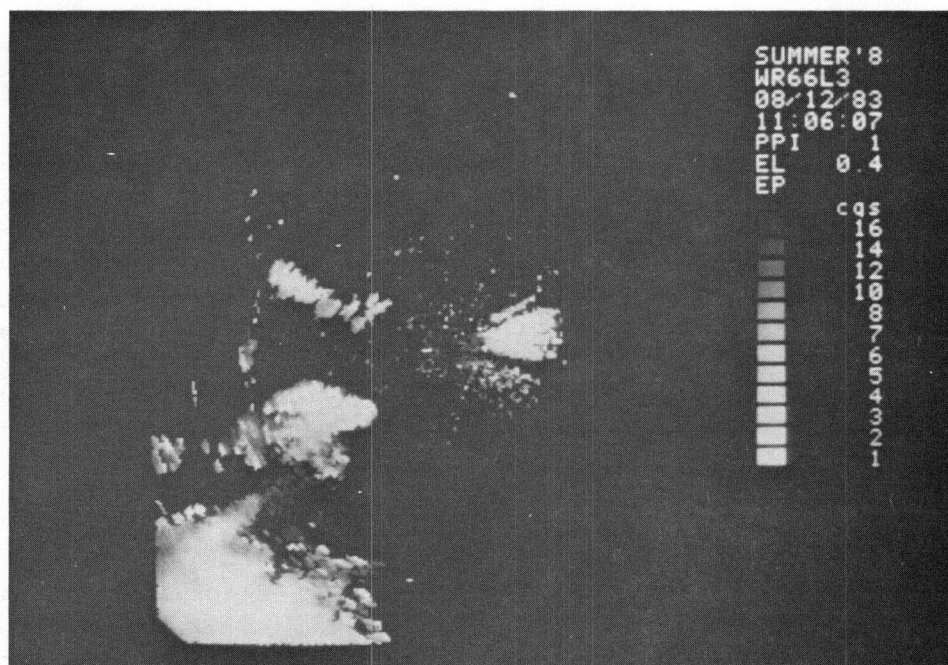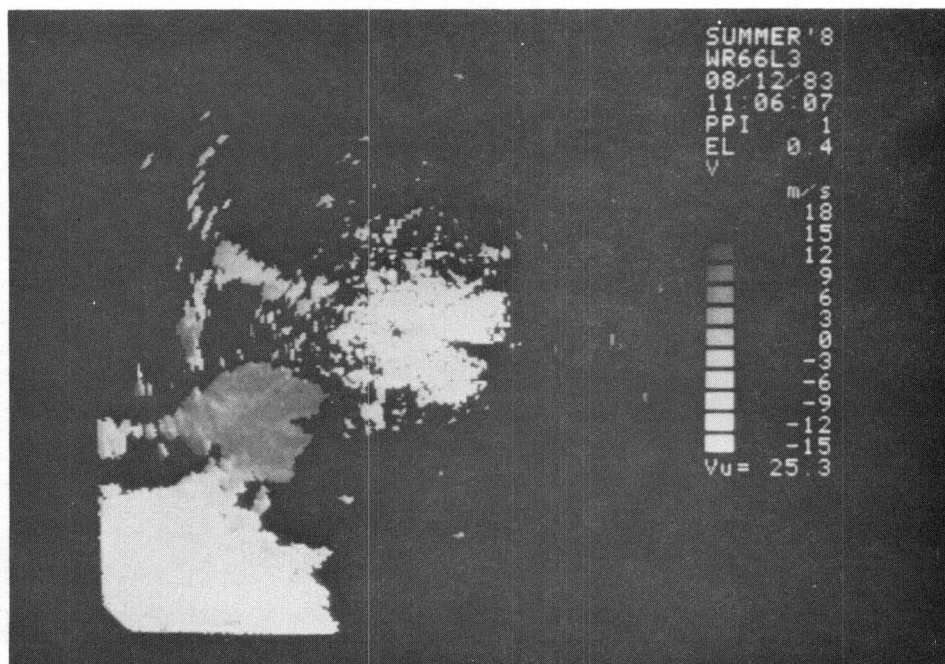
Figure 12.   PPI of (a) mean Doppler velocity (V in m/s) and (b) turbulence severity index (EP in $cm^{2/3} sec^{-1}$) for 1106 GMT 12 August 1983.

Another issue influencing spectrum width estimation is contamination due to illumination of extraneous scatterers. At low elevation angles, clutter can bias the spectrum width estimates as discussed in Zrnic' et al., (1983). Sidelobe illumination of storm features can place large spectrum widths in regions of light turbulence. Thus general structural information can be of value in interpreting the significance of large spectrum widths.

Point targets such as aircraft and birds and extraneous RF pulse interference can also cause significant bias errors in spectrum width estimation. The effect of such targets can be alleviated to some extent by filtering based on reflectivity/spatial signatures which are inconsistent with weather signals.

Finally, we remark that spectrum width estimation accuracy even in the absense of biasing influences is related in a complex way to several parameters including the width itself, the signal–to–noise ratio, and the number of weather samples used in the calculations. Other radar parameters such as the maximum unambiguous velocity are also important. Pulse pair estimators are based on a Gaussian weather spectrum assumption and become inaccurate for very narrow and very wide spectrum widths. Doviak and Zrnic'(1984) and the references cited therein should be consulted for quantitative details. We also note that there are data (Labitt, 1981; Janssen and VanDerSpek, 1985) indicating that weather spectra deviate from the Gaussian shape in a significant number of cases. Janssen and VanDerSpek (1985) state that this is true for 25% of the cases they analyzed.

3.5 Stationarity

As mentioned in a previous section, when computing the radar layered turbulence products, we assumed that the spatial distribution remained essentially constant over the period of a radar volume scan (the maximum time is about 5 minutes). From the analysis of the storm characteristics (i.e., storm size and vertical development), the pilot's report of cloud development, and the computed turbulence patterns for adjacent volume scans it seems reasonable to expect that the non–stationarity present on time scales on the order of the volume scan period did not seriously affect the turbulence estimates reported here. Figures 13, 14 and 15 show the reflectivity, spectrum width, and turbulence severity indices for three successive volume scans extending over an eleven minute period. While temporal development is evident, no large scale variations are noted.

3.6 Summary of Section 3

In summary, a common feature appearing in this study and in the study by Labitt (1981) is that radar $\epsilon_r^{1/3}$ values are much higher than corresponding aircraft estimates of $\epsilon_r^{1/3}$. The accuracy of Doppler radar–derived $\epsilon_r^{1/3}$ estimates is dependent upon the accuracy of second moment estimates and the assumptions made in the derivation of Eq. (8). The $\epsilon_r^{1/3}$ estimates calculated from Eq. (8) rely heavily on the assumptions of homogeneity and isotropy. These assumptions may not rigorously hold within thunderstorms, particularly in the regions of turbulence generation. The error in $\epsilon_r^{1/3}$ due to a lack of homogeneity is unknown. In addition, the neglect of wind shear contributing to spectrum widening may result in overestimates in $\epsilon_r^{1/3}$ particularly for light turbulence levels. Furthermore, owing to the fact that radar observations were not coordinated in time and
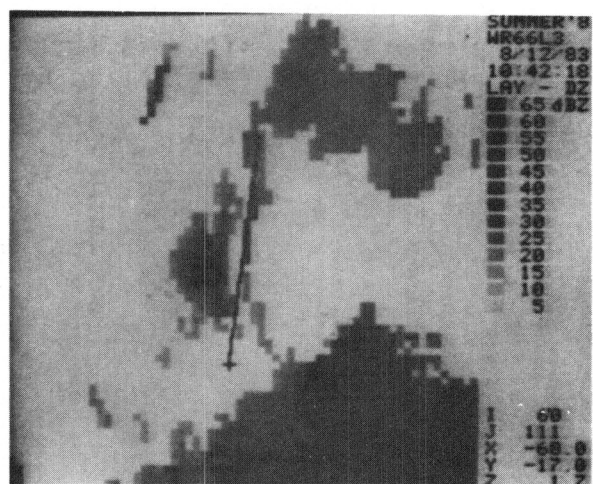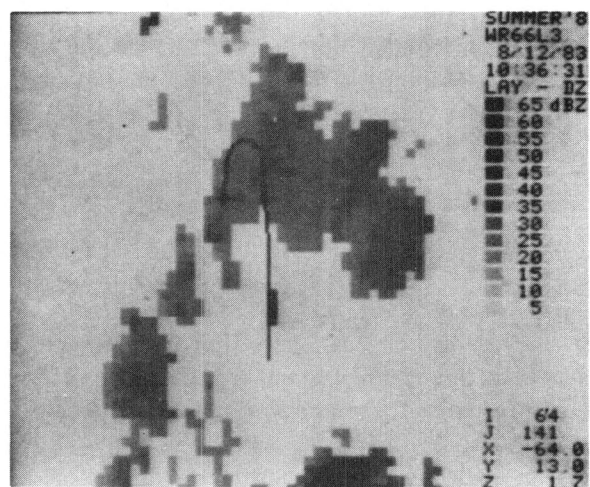
Figure 13. PPI of layered reflectivity (DZ in dBZ) at (a) 1031 GMT, (b) 1036 GMT and (c) 1042 GMT on 12 August 1983 illustrating the development of the storm.
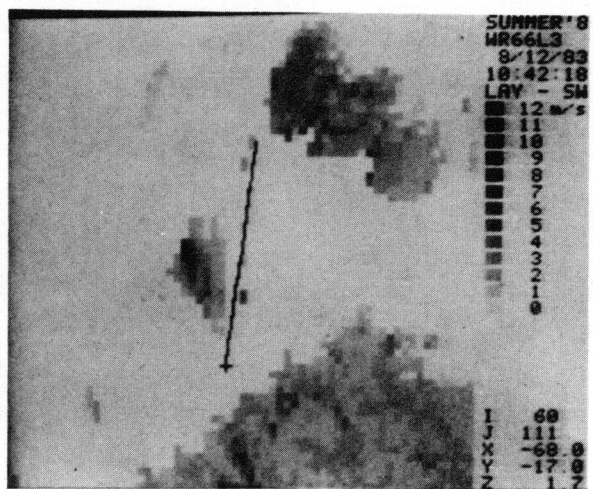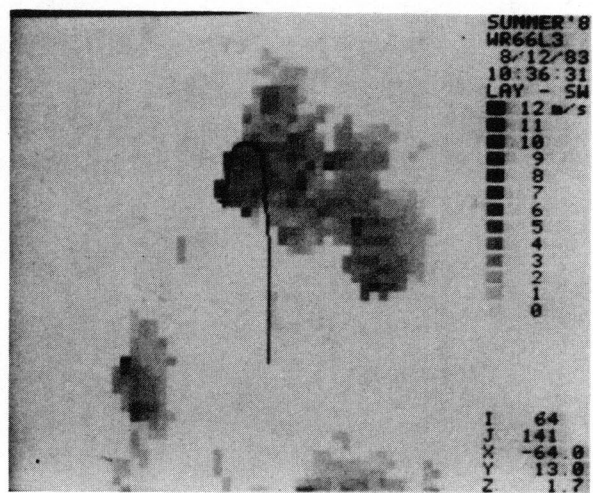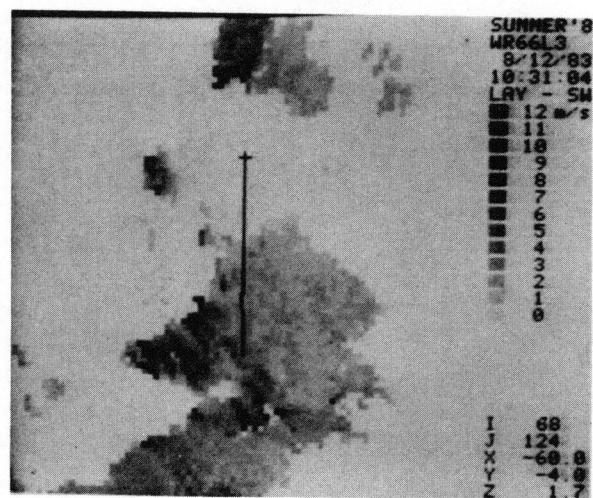
Figure 14. PPI of layered spectrum width (SW in m/s) at (a) 1031 GMT, (b) 1036 GMT and (c) 1042 GMT on 12 August 1983 illustrating the development of the storm.
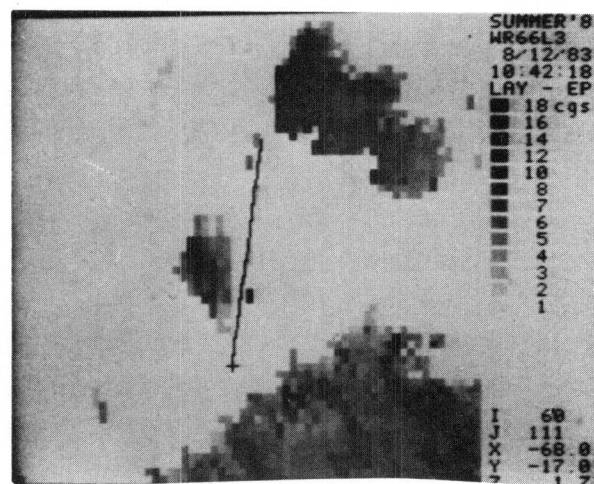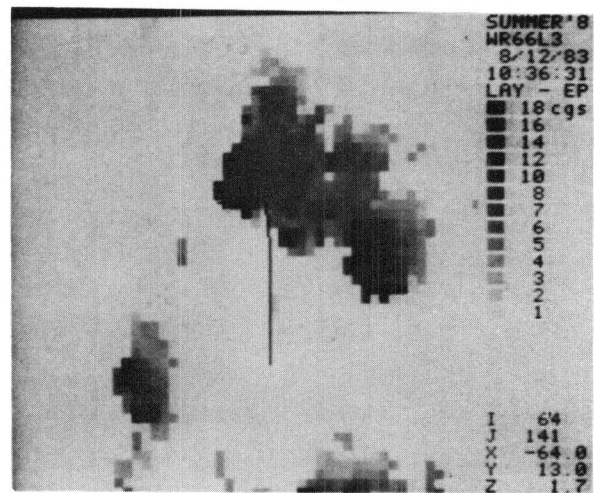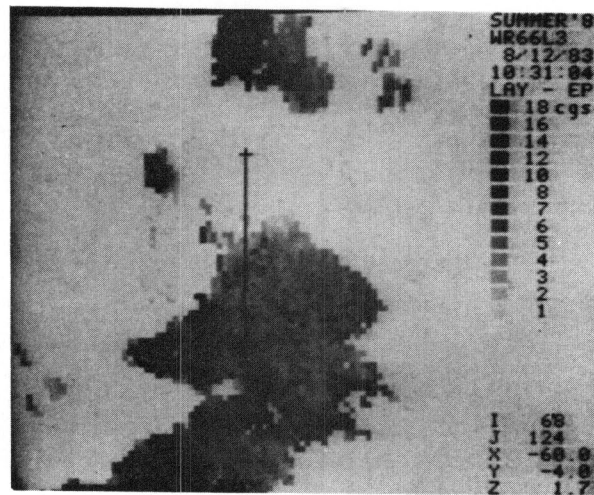
Figure 15. PPI of layered turbulence severity index (EP in cm$^{2/3}$ sec^{-1}) at (a) 1031 GMT, (b) 1036 GMT and (c) 1042 GMT on 12 August 1983 illustrating the development of the storm.

space with aircraft flight paths, temporal evolution of turbulent fields and turbulence-related meteorological parameters could have occurred between the times when the radar and aircraft sampled the general region. Thus, differences between the radar and aircraft $\epsilon^{1/3}$ values are not unexpected.

4. SPECTRUM WIDTH AS A TURBULENCE INDICATOR

Lee (1977) observed a strong connection between spectrum width and aircraft measurements of turbulence and recommended the use of spectrum width, σ_v, itself as the radar measure of turbulence. His data show that when aircraft-derived gust velocities, U_{de}, exceeded 6 m/sec, corresponding to moderate or heavy turbulence, the spectral width exceeded 5 m/sec in every case for aircraft within 1 km of the radar resolution volume.

Our results indicate that of the 404 minutes of useful data analyzed, none of U_{de} exceeded 6 m/sec. Meanwhile, examination of the spectrum width for all the flights show that, occasionally, σ_v exceeded 5 m/sec. For example, on the flight segment of 1530 GMT to 1600 GMT on 12 August 1983, σ_v occasionally exceeded 5 m/sec. In contrast, U_{de} never exceeded 2 m/sec for the same flight segment. The corresponding radar $\epsilon_r^{1/3}$ indicated heavy-to-extreme turbulence for almost the entire flight (see Figure 5). This feature appears in other cases shown in the figures contained in Volume II. This suggests that using spectrum width alone as a turbulence indicator would result in fewer false alarms as compared with the radar $\epsilon_r^{1/3}$. But it should be pointed out that a set of threshold values derived from spectrum width for various turbulence categories needs to be defined and validated. The development of such a set of thresholds is complicated by the fact that spectrum width is dependent on radar resolution volume size as well as turbulence intensity. Thus spectrum width is not an intrinsic measure of storm turbulence.

5. DISCUSSION AND SUMMARY

This report has presented turbulence related data based on aircraft observations and Doppler radar observations. Layered Cartersian turbulence maps were developed from radar estimates. Turbulence intensity was characterized by spectrum width, turbulence severity index derived gust velocity and subjective comments from the pilots who conducted the flights.

Almost all the flights were conducted at long range (*i.e.*, greater than 60 km) using a wider beam than NEXRAD (*i.e.*, 1.45°). The storms encountered were not very severe. In general, the radar estimates of turbulence severity index exceeded the aircraft estimates, sometimes by an order of magnitude. Overestimates were most significant in light turbulence cases. Radar estimates of turbulence, even when averaged over the largest layer size, preserved the general pattern of turbulence fluctuations. Stronger turbulence resulted in reasonable agreement between aircraft and radar estimates, although the radar estimates exceeded the aircraft estimates. Aircraft based dissipation rates also exceeded the level of turbulence indicated by subjective pilot's comments. Derived gust velocities always suggested significantly lower levels of turbulence intensity than did any of the dissipation rates estimates.

Due to the nature of the radar measurements there are two most likely causes for the discrepancy between the aircraft and radar measurements. The presence of shear may have dominated the spectrum width in light turbulence. The resolution volume size associated with most of the measurements may have been large enough that the assumptions associated with inertial subrange concepts (*i.e.*, homogeneity isotropy, and the limitations of finite outer scale) break down resulting in an invalid turbulence characterization.

This work has shown that while radar measurements provide a relative measure of turbulent activity, even when layered for FAA applications, the NEXRAD turbulence algorithm will result in false alarms when detecting long range light turbulence. Future work should focus on refining the algorithm in such a way that consistent radar turbulence maps can be developed which truly identify hazardous airspace. To this end, the interpretation of shear information must be examined and techniques for the judicious removal of non-hazardous shear contributions from spectrum width must be developed. More aircraft data are required in order to calibrate the radar turbulence measurements in terms of relative hazard. The use of storm structure information in the interpretation of turbulence measurements must be explored. More data from closer range flights are required to assess NEXRAD turbulence performance over the whole region of intended NEXRAD coverage. While spectrum width as a turbulence indicator depends on resolution volume size, its use as an empirical turbulence measure requires further evaluation.

6. CONCLUSIONS

1. This report provides the first comparison of aircraft turbulence measurements with Doppler weather radar estimates in which the radar volume scan data have been averaged horizontally and vertically to yield the layered Cartesian turbulence fields intended by the FAA for real-time ATC use by non-meteorologists (*e.g.*, pilots and controllers).

2. This initial analysis has revealed a number of uncertainties associated with the kinetic dissipation rate-based turbulence algorithm. In particular, the algorithm overstates the severity of hazard for the flights analyzed, regardless of the level of turbulence intensity. However, for moderate turbulence, the spread of the data is reduced. There were no encounters of severe or extreme turbulence in 1983, but data from 1985 and 1986 may yield such encounters.

3. The current NEXRAD turbulence algorithm with its refinements to Labitt's (1981) simpler model provides poorer agreement with the aircraft data than did Labitt's model.

4. Many features of the turbulence detection algorithm and operational use of the resulting product need to be reexamined. These include

   a. shear removal and signal-to-noise thresholding,

   b. adjustment of the magnitude of the proportional constant C associated with the energy spectrum/structure function,

   c. analysis of the aircraft and radar data to validate the fundamental concepts (e.g., isotropy, homogeneity, and Kolmogorov's formula) used in arriving at the kinetic dissipation rate as a turbulence indicator,

   d. use of spectrum width as an empirical turbulence measure, and

   e. consideration of a wider variety of turbulence detection approaches such as the use of storm structure in conjunction with spectrum width (or $\epsilon_r^{1/3}$).

REFERENCES

Anderson, J.: Evaluating ground filters for weather radars, *Preprints, 20th Conf. on Radar Meteor.*, Amer. Meteor. Soc., Boston, MA, pp. 314–318, (1981).

Bachelor, G. K.: The theory of homogeneous turbulence, University Press, Cambridge, UK, 197 pp., (1960).

Bohne, A. R.: Radar detection of turbulence in precipitation environments, *J. Atmos. Sci.*, 39, pp. 1819–1837, (1982).

Bohne, A. R.: In–flight turbulence detection, Air Force Geophysics Laboratory Technical Report AFGL–TR–85–0049, 55 pp. (1985).

Cadet, D.: Energy dissipation within intermittent clear air turbulence patches, *J. Atmos. Sci.*, 34, pp. 137–142, (1977).

Champagne, F. H., C. A. Friehe and J. C. LaRue: Flux measurements, flux estimation techniques and fine–scale turbulence measurements in the clustable surface layer over land, *J. Atmos. Sci.*, 34, pp. 515–530, (1977).

Doviak, R. and D. Zrnic': Doppler radar and weather observations, Academic Press, Inc., New York, NY, (1984).

Frisch, A. S. and S. F. Clifford: A study of convection capped by a stable layer using Doppler radar and acoustic echo sounders, *J. Atmos. Sci.*, 31, pp. 137–142, (1974).

Frisch, A.S. and R. G. Strauch: Doppler–radar measurements of turbulence kinetic energy dissipation rates in a northeastern Colorado convective storm, *J. Appl. Meteor.*, 15, pp. 1012–1017, (1976).

Gage, K. S.: Evidence for a K–5/3 law inertial range in mesoscale two–dimensional turbulence, *J. Atmos. Sci* ., 36, pp. 1950–1953, (1979).

Gossard, E. E., R. B. Chadwick, T. R. Stetman and J. Gaynor: Capability of surface–based clear–air Doppler radar for monitoring meteorological structure of elevated layers, *J. Climate Appl. Meteor.*, 23, pp. 474–485, (1984).

Janssen, L. and G. VanDer Spek: The shape of Doppler spectra from precipitation, *IEEE Trans–Aero. and Elect. Sys.*, Vol. AES–21, No. 2, pp. 208–219, (1985).

Labitt, M.: Coordinated radar and aircraft observations of turbulence, Project Report ATC–108, Lincoln Laboratory, MIT, (1981).

Laird, B. G.: On ambiguity resolution by random phase processing, *Preprints, 20th Conf. on Radar Meteor.*, Amer. Meteor. Soc., Boston, MA, pp. 327–331, (1981).

Lee, J. T.: Application of Doppler weather radar to turbulence measurements which affect aircraft, Final Report No. FAA–RD–77–145, Prepared for U.S. Dept. of Transportation, FAA Systems Research and Development Service, Washington, DC, (1977).

MacCready, P.: Standardization of gustiness values from aircraft, *J. Appl. Meteor.*, 3, pp. 439–449, (1964).

NEXRAD JSPO: NEXRAD Technical Requirements (NTR), R400-SP301, 263 pp., (1985).

Obukhov, A. M. and A. M. Yaglom: The microstructure of turbulent flow, *Prikl. Matem. i Mekh* , pp. 3-26 (in Russian), (1951).

Panchev, S.: Random functions and turbulence, Pergammon Press, New York, NY (1971).

Pratt, K. G. and W. G. Walker: A revised gust-load formula and a re-evaluation of U-G data taken on civil transport airplanes from 1933-1950, National Advisory Committee of Aeronautics Report 1206 , pp. 1-4, (1954).

Takeuchi, T.: On the nondimensional rate of dissipation of turbulenc energy in the surface boundary layer, *J. Meteor. Soc. Japan*, Ser. 2-40, pp. 127-135, (1962).

Thomas, D. D.: Turbulence related accidents: Worldwide synopsis, Final Report FAA Symposium on Turbulence, (1971).

Turner, E. W., J. C. Sims and A. White: Categorization of atmospheric turbulence in terms of aircraft response for use in turbulence reports and forecasts, Flight Dynamics Laboratory, Wright-Patterson AFB, Ohio, Final Report AFWAL-TR-81-3058, (1980).

Zrnic', D., S. Hamidi and A. Zahrai: Considerations for the design of ground clutter cancelers for weather radar, Final Report No. FAA-RD-82-68, Prepared for U.S. Dept. of Transportation, FAA Systems Res. and Develop. Serv., Washington, DC, (1983).